

Adaptive Replication Strategies in Trust-Region-Based Bayesian Optimization of Stochastic Functions

Mickaël Binois^a and Jeffrey Larson^b

^aInria, Université Côte d’Azur, CNRS, LJAD, Sophia Antipolis, France.

`mickael.binois@inria.fr`

^bMathematics and Computer Science Division, Argonne National Laboratory.

`jmlarson@anl.gov`

Abstract

We develop and analyze a method for stochastic simulation optimization based on Gaussian process models within a trust-region framework. We focus on settings where the variance of the objective function is large, making accurate estimation challenging and often requiring many evaluations. To address this regime, we combine local modeling with adaptive replication, allowing the method to allocate repeated evaluations where they are most beneficial. We introduce several mechanisms to promote and adapt replication, including modifications to the acquisition function and cost-aware evaluation strategies. These components enable our approach to scale effectively when high levels of sampling are required to reduce noise. Numerical experiments show that adaptive replication can substantially improve solution accuracy by several orders of magnitude over baseline methods and computational efficiency when evaluation costs are taken into account.

Keywords: *Gaussian processes; Trust-region methods; Input-varying variance; Setup costs*

1 Introduction

We consider the optimization of a stochastic oracle or function $y : D \subset \mathbb{R}^d \mapsto \mathbb{R}$, where evaluations of y are accessible only through noise-corrupted evaluations, $y(\mathbf{x}) \triangleq f(\mathbf{x}) + \epsilon(\mathbf{x})$, where $\epsilon(\mathbf{x})$ is a random variable with mean zero and finite variance $r^2(\mathbf{x})$. In practice, $r^2(\mathbf{x})$ may be unknown, and we assume that the noise is Gaussian. Because $y(\mathbf{x})$ is stochastic, relying on single samples is typically insufficient for determining the underlying function value. Instead, we will have to sample $y(\mathbf{x})$ multiple times in order to solve the problem:

$$\text{find } \mathbf{x}^* \in \arg \min_{\mathbf{x} \in D} \mathbb{E}[y(\mathbf{x})]. \quad (1)$$

We assume that the cost of evaluating $y(\mathbf{x})$ is nontrivial and therefore seek methods that require the fewest possible oracle queries to solve (1). Given the probabilistic nature of this optimization problem, we seek to solve it using probabilistic models, namely, Gaussian processes (GPs). Among surrogate models, GPs are used for their prediction accuracy and analytic tractability, plus their ability to handle multi-modality. More importantly, they offer robust uncertainty quantification and effective noise filtering, both of which are critical for stochastic optimization.

A possible strategy for separating signal from noise in (1) is to fix a number of replications/evaluations of y to be performed at any \mathbf{x} requested by the optimization method [30, 43]. This simplification is useful when

the signal-to-noise ratio is low, but it may be wasteful away from portions of the domain D that are critical to optimization. Limited research has been conducted on methods that adaptively control the number of replicates. This control can be achieved either by allowing the method to determine the number of replicates when selecting new points (single stage) or by including a replication phase (in multistage approaches); see, for example, [30, 49]. In this work we focus on adaptively managing replication when proposing new points, the single-stage case, so that the overall evaluation budget is more effectively distributed across the parameter space. Such a replication approach is also beneficial when using GP surrogates because it reduces the associated computational cost of updating the GP with new observations. These updates can quickly become a bottleneck when the total number of oracle evaluations grows (something that is needed to converge precisely). Using relatively larger evaluation budgets is referred to as the high-throughput regime in BO, which also involves parallel evaluation (e.g., of replications) [45].

Although our framework is general, this work is motivated by an application where the cost of evaluating $y(\mathbf{x})$ incurs a setup cost that is paid only once for all subsequent replications. Specifically, the cost of obtaining p evaluations of y at \mathbf{x} is $c(p) \triangleq c_0 + c_1 \times p$. Note that the cost c_0 is incurred any time replications are requested, so obtaining an appropriate p is important. That is, twice querying y at \mathbf{x} for a single replication costs $2(c_0 + c_1)$; but if it is known that two replications are desired, the cost can be reduced to $c_0 + 2c_1$. Such a cost structure arises when optimizing variational circuit parameters for quantum computing applications where preparing the circuit cost (c_0) is approximately 100 to 1000 times more expensive than observing one sample (or “shot”) of the system [36].

Such a model emphasizes the need to balance setup costs with the number of replications; this is similar to the “cost-aware Bayesian optimization” community (see, e.g., [22, 32]) where the goal is to balance evaluation cost and the regret—the difference between the objective value at the returned solution and the optimal value. This related (but distinct) problem occurs when the evaluation cost function depends on \mathbf{x} (see, e.g., [54, 55]). Such a cost/benefit trade-off is also present with multifidelity objectives, where evaluations at different fidelity levels have different evaluation costs impacting the accuracy. In these situations, some researchers have developed acquisition functions that jointly select the next point and fidelity level; see [29, 31, 58]. This approach may be an option if limiting to a few possible replication budgets per observation. Lifting this restriction to use only a few possible fidelity levels, Kandasamy et al. [31] proposed a continuous version with a GP on both D and fidelity level. In the presence of stochastic noise where fidelity corresponds to the number of replicates, however, this setup effectively reduces to a noisy GP model [50]. Most of these techniques have been explored in either deterministic or high signal-to-noise regimes, highlighting the need for novel methods tailored to the demanding scenario of high variance, rapid convergence requirements, and nontrivial setup costs.

To this end, we utilize a trust-region (TR) framework. TR methods provide a systematic way to explore the domain by iteratively refining a localized region around promising candidates, and they can be paired with different surrogate models. The appeal of this combination has been demonstrated in recent works. For instance, TRs have been employed with polynomials [33, 60], radial basis functions [66, 67] and, more recently, Gaussian processes [1, 18, 20, 47, 57], although most of these GP studies assume a deterministic f or a high signal-to-noise regime. The difficulty is that when reducing the TR radius, the signal-to-noise ratio decreases as well. Lower signal-to-noise ratios have been explored by the operations research community [43, 49], often with stochastic kriging models [2], which can identify solutions near a local optimum but rarely achieve high

precision using only GPs. That is, these methods have difficulty finding solutions with regret considerably less than the noise level. They also do not jointly find the next point and evaluation budget; in other words, they are not single-stage methods. Some researchers propose switching to a different optimizer (e.g., [42]) or adopting a strategy that discards GPs in the local search [40, 46]. Here we focus on improving the GP-based local search.

In order to accommodate noise, possibly with a heteroscedastic variance, and potential non-stationarity in the objective, one option is to transform inputs and outputs, as in [17] with learnable parametric transformations of the input and output spaces. Another option is to employ local models [26] combined with replication, a path we pursue because it can significantly reduce computational overhead. This approach is particularly well suited to the high-noise regime in which repeated evaluations at promising points are essential for accuracy, yet overall evaluation budgets remain limited.

Our main contributions are fourfold. First, we rely on replication and adaptively control the number of replicates when selecting new points. This strategy may be governed by the evaluation cost problem structure. Second, we make key modifications to the standard GP trust-region framework to handle low signal-to-noise ratios. Third, we propose a trust-region method built on local GP models that scales efficiently with the large number of observations required for high accuracy. Fourth, we provide software demonstrating superior performance and scalability against other methods on a range of test problems.

We do not seek to formally establish convergence guarantees or rates for the modified algorithm. The underlying GP and trust-region frameworks that we are building on have almost-sure convergence results (say, under suitable regularity assumptions for the GP, acquisition function and local search, see e.g., [65, 68], or [22, Ch. 10]). Our modifications are designed to preserve almost-sure convergence guarantees of these methods while improving their practical performance in noisy and high-throughput regimes. Also, asymptotic convergence behavior is rarely observed in practical finite-budget settings. This further motivates our emphasis on performance and robustness rather than asymptotics.

2 Formalization

This section presents background information on Gaussian processes, Bayesian optimization, and trust-region methods.

2.1 Gaussian process regression

Assuming that $\epsilon \sim \mathcal{N}(0, r^2(\mathbf{x}))$ for simplicity, we model y by a prior zero-mean Gaussian process Y with a covariance function k . Given N observations $\mathbf{y} \triangleq (y_i)_{1 \leq i \leq N}$ at $\mathbf{x}_1, \dots, \mathbf{x}_N$, following standard textbooks (e.g., [25, 56]), the prediction at any given \mathbf{x} is $Y(\mathbf{x})|\mathbf{y} \sim \mathcal{N}(m_N(\mathbf{x}), s_N^2(\mathbf{x}))$ with mean and variance given by

$$m_N(\mathbf{x}) \triangleq \mathbb{E}[Y(\mathbf{x})|\mathbf{y}] = \mathbf{k}(\mathbf{x})^\top (\mathbf{K}_N + \mathbf{\Lambda}_N)^{-1} \mathbf{y}, \quad (2)$$

$$s_N^2(\mathbf{x}) \triangleq \mathbb{V}[Y(\mathbf{x})|\mathbf{y}] = r^2(\mathbf{x}) + k(\mathbf{x}, \mathbf{x}) - \mathbf{k}(\mathbf{x})^\top (\mathbf{K}_N + \mathbf{\Lambda}_N)^{-1} \mathbf{k}(\mathbf{x}), \quad (3)$$

where $\mathbf{\Lambda}_N \triangleq \text{Diag}(r^2(\mathbf{x}_1), \dots, r^2(\mathbf{x}_N))$, $\mathbf{k}(\mathbf{x}) \triangleq (k(\mathbf{x}, \mathbf{x}_j))_{1 \leq j \leq N}$ and $\mathbf{K}_N \triangleq (k(\mathbf{x}_i, \mathbf{x}_j))_{1 \leq i, j \leq N}$. Since the noise has mean zero, the corresponding GP model for f is such that $\mathbb{E}[f(\mathbf{x})|\mathbf{y}] = m_N(\mathbf{x})$ while $\mathbb{V}[f(\mathbf{x})|\mathbf{y}] =$

$k(\mathbf{x}, \mathbf{x}) - \mathbf{k}(\mathbf{x})^\top (\mathbf{K}_N + \mathbf{\Lambda}_N)^{-1} \mathbf{k}(\mathbf{x})$. There exist extensions to non-Gaussian noise, and therefore non-Gaussian likelihood, requiring additional approximations; see, for example, [28]. In the remainder of this paper we focus on the Gaussian noise framework.

A useful tool in this context is replication, that is, repeating experiments at the same \mathbf{x}_i . In this Gaussian framework, a_i evaluations at $\mathbf{x}_i, y_i^{(1)}, \dots, y_i^{(a_i)}$, give an equivalent Gaussian observation with mean $\bar{y}_i \triangleq \frac{1}{a_i} \sum_{j=1}^{a_i} y_i^{(j)}$ and variance $r^2(\mathbf{x}_i)/a_i$. If a_i is large enough, then the empirical mean and variance give good approximations of $f(\mathbf{x}_i)$ and $r^2(\mathbf{x}_i)$. Hence, by controlling a_i , one can control the variance of the equivalent aggregated observation. The benefits are as follows:

- The output of the algorithm is one $(\mathbf{x}_i, \bar{y}_i)$ with variance smaller ($a_i > 1$) than or equal ($a_i = 1$) to that of a single evaluation.
- Replicating brings speedups for GPs by using the equivalent observations, lowering the $\mathcal{O}(N^3)$ complexity to $\mathcal{O}(n^3)$ with n the number of unique \mathbf{x}_i s.
- $r^2(\mathbf{x}_i)$ is easier to estimate, since the empirical variance may be computed.

In the heteroscedastic output noise variance case, by denoting the number of replicates at observed locations with $\mathbf{A}_n \triangleq \text{Diag}(a_1, \dots, a_n)$, we can give the GP prediction for y equivalently by

$$m_n(\mathbf{x}) \triangleq \mathbf{k}(\mathbf{x})^\top (\mathbf{K}_n + \mathbf{\Lambda}_n \mathbf{A}_n^{-1})^{-1} \bar{\mathbf{y}}, \quad (4)$$

$$s_n^2(\mathbf{x}) \triangleq r^2(\mathbf{x}) + k(\mathbf{x}, \mathbf{x}) - \mathbf{k}(\mathbf{x})^\top (\mathbf{K}_n + \mathbf{\Lambda}_n \mathbf{A}_n^{-1})^{-1} \mathbf{k}(\mathbf{x}). \quad (5)$$

In the remainder, depending on the context, we will use either the generic full- N notation or the replicate- n one (dropping the dependence on \mathbf{A}_n in a slight abuse of notation).

The covariance function k is typically selected from a parametric family, such as the Gaussian or Matérn covariance functions. Here we use the Matérn 5/2 covariance function:

$$k(\mathbf{x}, \mathbf{x}') = \sigma^2 \prod_{i=1}^d \left(1 + \frac{\sqrt{5}|x_i - x'_i|}{l_i} + \frac{5(x_i - x'_i)^2}{3l_i^2} \right) \exp \left(-\frac{\sqrt{5}|x_i - x'_i|}{l_i} \right)$$

with parameters σ^2 for the process variance and lengthscales l_i . Most packages propose learning these hyperparameters based on the likelihood. When the $r^2(\mathbf{x}_i)$ are unknown, they need to be estimated as well, which can be difficult. A naive way is to just estimate a constant noise, which is sensible if the trust region is small enough. Alternatives for learning r^2 include stochastic kriging [2] and likelihood-based approaches [7]. Once fitted, the GP model can be employed for optimization.

2.2 Bayesian optimization

For a broad overview of derivative-free optimization, we refer the reader to [35]. Within this field, Bayesian optimization (BO) is a powerful framework that uses a probabilistic surrogate—often a Gaussian process—to model the objective function [22]. At each iteration, an *acquisition function* (or *infill criterion*) determines where to sample next, balancing *exploration* of regions of parameter space with high predictive variance against *exploitation* of regions of parameter space with low predictive mean. By updating the surrogate

model with each new observation, BO adapts its search strategy and efficiently converges to high-quality solutions, even in noisy or expensive-to-evaluate settings.

Common acquisition functions are based on the notion of improvement, that is, the random variable $I(\mathbf{x})|\mathbf{y} \triangleq \max(0, T_n - Y(\mathbf{x})|\mathbf{y})$, where T_n is the best observed value in the deterministic case (i.e., $T_n = \min_{1 \leq i \leq n} y_i$). This leads to the probability of improvement or the expected improvement (EI): $EI(\mathbf{x}) \triangleq \mathbb{E}[I(\mathbf{x})|\mathbf{y}]$. Both have closed-form expressions, but the latter is generally preferred, specifically:

$$EI(\mathbf{x}) = (T_n - m_n(\mathbf{x}))\Phi\left(\frac{T_n - m_n(\mathbf{x})}{s_n(\mathbf{x})}\right) + s_n(\mathbf{x})\phi\left(\frac{T_n - m_n(\mathbf{x})}{s_n(\mathbf{x})}\right), \quad (6)$$

where ϕ and Φ are the probability and cumulative density functions of the standard Gaussian distribution, respectively. For notational simplicity, next we drop the implicit conditioning on the current data, \mathbf{y} .

In the stochastic setting, T_n is typically the best predictive mean over all observations [25] (i.e., $T_n = \min_{1 \leq i \leq n} m_n(\mathbf{x}_i)$). We follow this plugin approach here, which simplifies computation of the acquisition function. More Bayesian versions are included in [37], and detailed discussions are provided by [25, 7.2], [22, 8.2]. Accounting for all the uncertainty in the improvement, both on the reference T_n if taken as the best solution and on GP prediction, computations link to those of a discretized knowledge gradient (KG); see, for example, [22, 52]. KG is a less myopic option than EI: $KG(\mathbf{x}) \triangleq \mathbb{E}[\min_{\mathbf{x}} m_n(\mathbf{x}) - \min_{\mathbf{x}} m_{n+1}(\mathbf{x})]$. However, this criterion has no analytical expression, which incurs a larger computational cost and the need for approximations.

Other noisy adaptations have been proposed, such as with the augmented expected improvement (AEI) [29, 30]: $AEI(\mathbf{x}) \triangleq EI(\mathbf{x})\left(1 - \frac{r(\mathbf{x})}{s_n(\mathbf{x})}\right)$ with T_n taken from a best predictive quantile. The second term leads to the ratio of the reduction in the posterior standard deviation after a new replicate is added, but only at the current best point. It thus takes into account the effect of replication, although indirectly through $s_n(\mathbf{x})$, as noticed in [52].

Yet another variant of EI, also taking into account the effect of a new observation, is the conditional improvement (CI), that is, the improvement at a reference location \mathbf{x} after another location \mathbf{x}_{n+1} is added [25]: $CI(\mathbf{x}, \mathbf{x}_{n+1}) \triangleq I(\mathbf{x}|\mathbf{x}_{n+1})$. The expected conditional improvement (ECI) is expressed as

$$\begin{aligned} ECI(\mathbf{x}) &\triangleq \mathbb{E}[CI(\mathbf{x})|\mathbf{y}] \\ &= (T_n - m_n(\mathbf{x}))\Phi\left(\frac{T_n - m_n(\mathbf{x})}{s_{n+1}(\mathbf{x})}\right) + s_{n+1}(\mathbf{x})\phi\left(\frac{T_n - m_n(\mathbf{x})}{s_{n+1}(\mathbf{x})}\right). \end{aligned} \quad (7)$$

Note that this is almost EI but using the future variance as if \mathbf{x}_{n+1} was observed, since s_{n+1} does not depend on the observations (see Eq. (5)). ECI is generally integrated over the input domain, leading to the integrated expected conditional improvement (IECI) that depends only on \mathbf{x}_{n+1} . But it is computationally costly since the spatial integral is not in closed form.

The main issue of EI is that it is myopic: it is optimal for a single new evaluation, but it does not take into account the effect of future evaluations nor of replication. So does another popular infill criterion, based on an upper confidence bound (UCB, for maximizing), $UCB(\mathbf{x}) \triangleq m_n(\mathbf{x}) - \beta s_n(\mathbf{x})$ with a tunable parameter β . One might also use the entropy of the minimizer value or location, which is sample efficient but generally computationally costly.

Developed for noisy optimization, the expected quantile improvement (EQI) has several appealing prop-

erties [51]. It looks at a given level $\beta \in [0.5, 1)$ of GP quantile $q_n(\mathbf{x}) = m_n(\mathbf{x}) + \Phi^{-1}(\beta)s_n(\mathbf{x})$, and the improvement is taken over the decrease of the β -quantile brought by a new observation at \mathbf{x}_{n+1} . The resulting expression is similar to that of EI, Eq. (6), where $T_n = \min_{1 \leq i \leq n} q_n(\mathbf{x}_i)$, while $m_n(\mathbf{x})$ and $s_n(\mathbf{x})$ are replaced by their counterparts for q_{n+1} , also in closed form. Depending on the level β and the noise of the future observation, EQI can suggest to replicate. Tuning the value of the future noise is also discussed by [51]; the proposed strategy is to consider that in the search of \mathbf{x}_{n+1} , all the remaining budget will be used there. In fact a fixed elementary budget is used at each iteration. A more dynamical procedure is to keep replicating until the value of the EQI becomes less than a fraction of its initial value, before selecting a new point. A limitation is that the next point is chosen based on a virtual replication number; hence it is not really single stage.

Extensions of these works to select batches of new points have been proposed; see, for example, [11, 15] and references therein. Most, however, do not take into account the option to replicate.

We illustrate in Figure 1 two criteria on two different setups with different signal-to-noise ratios. KG and EQI behave differently: KG wants new points on either side of the current local optima, while EQI wants to add points on them. The diminishing returns effect of adding more replicates is also visible on both criteria: the difference between curves for 1 and 10 replicates is much larger than for 100 and 1000 replicates.

2.3 TR methods and combination with BO

Trust regions have been used in various optimization strategies, for example with mesh-adaptive direct search [3]. The driving mechanism of TR methods is the control of the trust-region radius over iterations. In case progress is made, the radius can grow, whereas it is reduced otherwise. Several combinations of BO with trust regions have been proposed in the literature and have attracted attention in benchmarks; see, for example, [18, 20, 57, 59]. A possible motivation for such attention is that TR framework promotes more precise local convergence while still allowing for global exploration capabilities using a global Bayesian model.

Derivative-free optimization (DFO)-TR methods maintain a surrogate model $m_n(\mathbf{x})$ of the objective in the neighborhood $\mathcal{B}(\mathbf{x}_n, \Delta_n)$ centered at the current iterate \mathbf{x}_n with radius Δ_n . The model is constructed using previously sampled points and is designed to satisfy geometric (poisedness) conditions that ensure m_n it is sufficiently close to f on $\mathcal{B}(\mathbf{x}_n, \Delta_n)$. Each iteration, a trial step \mathbf{s}_n is computed by (approximately) minimizing

$$\min_{\|\mathbf{s}\| \leq \Delta_n} m_n(\mathbf{x}_n + \mathbf{s}).$$

This step is accepted (and $\mathbf{x}_{n+1} \leftarrow \mathbf{x}_n + \mathbf{s}$) or is rejected ($\mathbf{x}_{n+1} \leftarrow \mathbf{x}_n$) based on the ρ_n ratio of actual decrease over predicted decrease. When the objective is stochastic, values in the numerator must be replaced by estimates. If ρ_n is sufficiently large, Δ_n can be increased; otherwise, the step is rejected and Δ_n is reduced. Under suitable model accuracy conditions (e.g., fully linear or fully quadratic models), this framework yields global convergence to first- or second-order stationary points

When the objective is stochastic, the acceptance ratio ρ_n becomes a random quantity, and noise can lead to incorrect step acceptance or rejection. Model construction is also more delicate: regression models must balance bias and variance, and sample sizes may need to increase as $\Delta_n \rightarrow 0$ to ensure sufficient model accuracy relative to the trust-region radius. Estimating predicted reduction and enforcing sufficient decrease

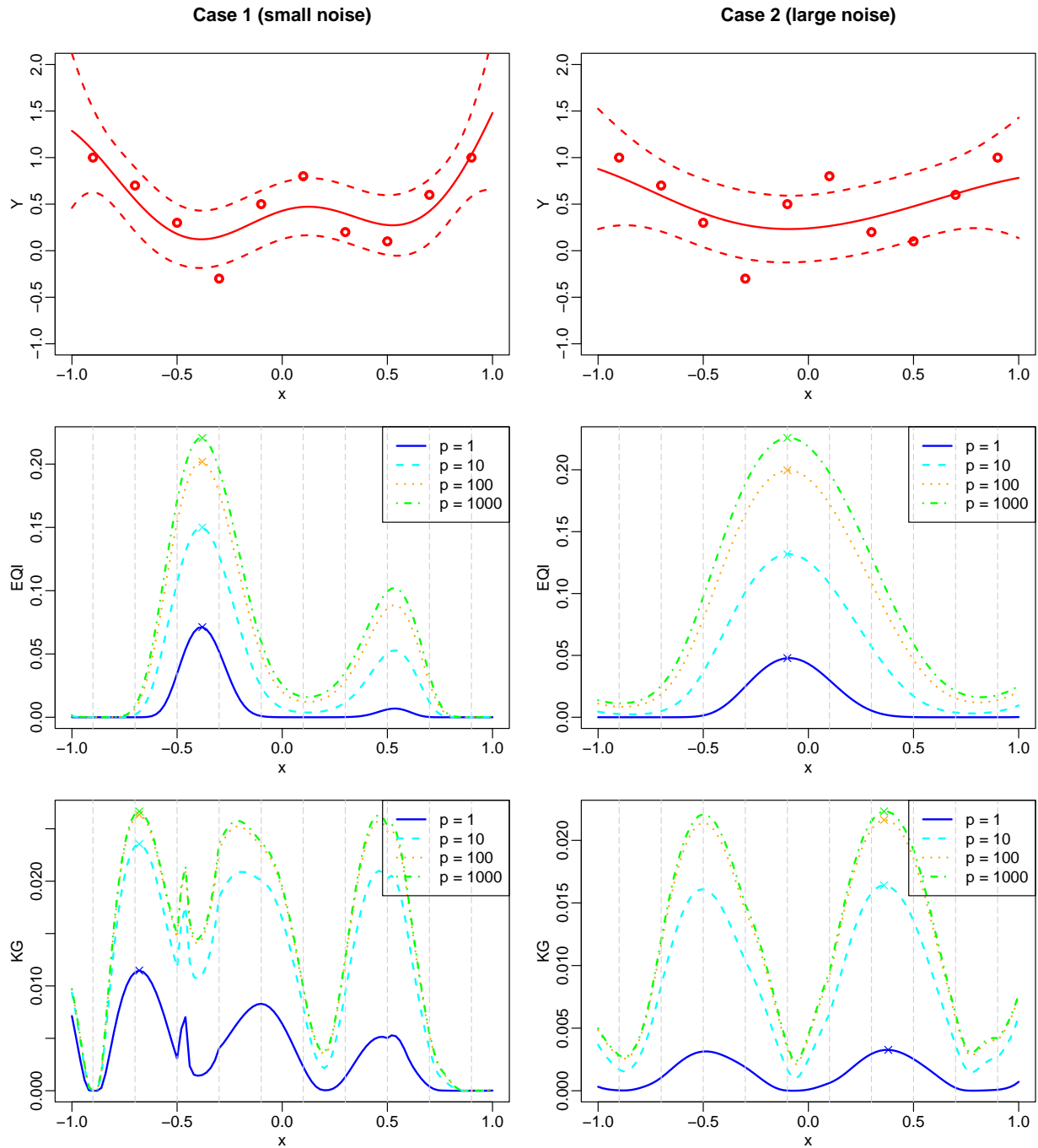


Figure 1: GP models and the KG and EQI infill criteria, depending on the number of replicates (p) at the future points, for two cases (left and right). Vertical lines indicate design points. Crosses mark the respective maxima.

conditions require variance-aware criteria. This can involve repeated sampling or adaptive sampling rules. Without careful control of noise (e.g., increasing sample sizes, using common random numbers, or employing probabilistic acceptance tests) the algorithm may stall at suboptimal points Stochastic DFO-TR methods

must couple model fidelity, sampling effort, and radius control to maintain both convergence guarantees and practical efficiency.

The differences between these methods depend on the balance between the two frameworks. The globalization strategy is either via global BO steps with local TR ones with TREGO [18], entertaining several trust regions in TuRBO [20], or performing restarts with TRIKE [57] or GSTAR [49]. The other main difference is on the success condition, which can be based on the actual improvement over EI, consecutive successes/failures, or a sufficient decrease condition. The infill criterion in the local steps also varies, from the predictive mean to EI or Thompson sampling. More local GP methods have proposed criteria based on the probability of descent; see, for example, [47]. The convergence rates for local BO are derived in [68].

Most of these do not deal specifically with the noisy setup. SNOWPAC [43] does, improving a polynomial surrogate by a GP one, also for constrained optimization, but it relies on the computation of a robustness measure obtained by sampling. Note that SNOWPAC requires a measure of the magnitude of the noise in the objective, something is not available in many situations we consider. For noisy simulator, GSTAR [49] relies on an ensemble of global and local GP models similar to stochastic kriging. But it remains in a two stage frameworks: new designs are added with a fixed number of replicates while more replicates are added to already sampled points in a dedicated phase.

3 Exploration-exploitation-replication trade-off

With this background information, we can now provide greater detail about our approach to decide both the next iterate \mathbf{x}_{n+1} and its associated number of replicates a_{n+1} . We also propose a new infill criterion, borrowing from links between batch and look-ahead formulations to handle the setup cost case.

3.1 Replication

First, as seen in (4), using replicates can directly lower the computational expense of model building. Without replication, to lower computational cost with large N , GP modeling often relies on techniques such as pseudo-inputs for sparse GPs [62], specialized linear algebra methods [64], or the Vecchia approximation [13]. In the low signal-to-noise regime, however, single evaluations offer limited information, and the overhead of deciding on a new point for just one evaluation may not be justified. An alternative is parallel/batch acquisition functions to evaluate multiple points simultaneously, but this introduces a more demanding optimization and approximation problem. In many cases, choosing a single new point with an appropriate replication budget proves both simpler and more effective.

Second, replication can be warranted by the acquisition function itself. In deterministic settings, this possibility does not arise; but in stochastic contexts, previous works have demonstrated that replicating at a single location can be optimal for certain global accuracy criteria (e.g., integrated mean square prediction error [10]) or for the EQI criterion [51].

Replication is still not the panacea. As the number of replicates increases, the marginal benefit diminishes because the noise standard deviation decreases in proportion to the square root of the number of replicates (see also Figure 1). Thus, finding the right replication level is critical. As detailed below, this decision can stem directly from the acquisition function or incorporate user-defined incentives such as a setup cost function. At a higher level, strategies include revisiting previously evaluated points to add a fixed number

of replicates [30], i.e., two-stage approaches, or enforcing a minimal distance between points [10]. Discrete domains also naturally lend themselves to replication because they prevent adding points arbitrarily close to one another, as may occur in continuous spaces.

Handling low signal-to-noise ratios often requires further adaptations, and incorporating these ideas into a trust-region framework brings additional subtleties. We address these considerations in the subsequent sections.

3.2 Looking ahead

The most common infill criteria—such as EI or UCB—do not naturally suggest a replication level for a given point because they account only for existing observations, not the number of future replicates. One might divide by an evaluation cost function that depends on \mathbf{x} [63], but that approach is outside our current scope. A more direct remedy is to adopt a look-ahead perspective, where policies consider the effect of p future observations at points $\mathbf{x}_{N+1}, \dots, \mathbf{x}_{N+p}$, shortened in $\mathbf{x}_{(N+1):(N+p)}$. In the GP context, closed-form update formulas [16, 25] facilitate such approaches. For example, adding $a_{n+1} = p$ replicates at \mathbf{x}_{n+1} updates the GP mean and variance as follows:

$$m_{N+p}(\mathbf{x}) = m_{n+1}(\mathbf{x}) = m_n(\mathbf{x}) + \frac{s_n^2(\mathbf{x}, \mathbf{x}_{n+1})}{s_n^2(\mathbf{x}_{n+1}) + r^2(\mathbf{x}_{n+1})/p} (\bar{y}_{n+1} - m_n(\mathbf{x}_{n+1})), \quad (8)$$

$$s_{N+p}^2(\mathbf{x}) = s_{n+1}^2(\mathbf{x}) = s_n^2(\mathbf{x}) - \frac{s_n^2(\mathbf{x}, \mathbf{x}_{n+1})^2}{s_n^2(\mathbf{x}_{n+1}) + r^2(\mathbf{x}_{n+1})/p}. \quad (9)$$

These update formulas have largely been used in look-ahead infill criteria—such as KG or entropy-based metrics—because the predictive variance term remains independent of the actual future observations, even though the predictive mean does not. However, fully propagating uncertainty from potential future samples makes look-ahead methods computationally challenging beyond a few steps. Various approximations therefore arise in practice [22, 23]. One strategy is to restrict the set of future decisions, for example by allowing only one new point in a future step and devoting all other steps to replication [10]. In that scenario, if adding a new point is more advantageous in a later iteration, then replication at \mathbf{x}_{n+1} is optimal for now—thus balancing exploration, exploitation, and replication.

But we can also rely on the “strong connection between the optimal batch and sequential policies” [22], such that a batch policy is a reasonable approximation of the sequential/look-ahead one. An example can be found in the GLASSES method [24].

3.3 Blending all together: a new infill criterion geared to trust-region methods

We primarily focus on *improvement-based* infill criteria rather than, for example, selecting iterates using only the predictive mean m_n . In our experience, the predictive mean in high-noise settings becomes relatively flat, often placing its minimum near the trust-region center \mathbf{x}_c . By contrast, improvement-based methods foster more exploration.

Our approach here will take advantage of the closed-form expression for the future predictive variance without explicitly modeling the noisy future observations, thereby retaining computational efficiency. One criterion meeting this requirement is IECI, although it involves a costly spatial integral.

Our novel infill criterion is qERCI, for parallel expected reduction in conditional improvement. More precisely, we consider the reduction in improvement at several reference locations brought by a batch of candidate evaluations. The rationale is that in a TR framework, besides the new point(s), the main points of interest are the current center \mathbf{x}_c , the estimated optimum \mathbf{x}_n^* (which can coincide with the center, but not necessarily). A key point is that we want to estimate it a priori, among existing points, not a posteriori as with KG, which would become more computationally expensive. Plus in high-noise regimes, where the GP prediction is comparatively flat (see Figure 1), preliminary estimates of the minimum value and location based on the predictive mean appearing in the acquisition function are unlikely to change drastically once the new observations are incorporated.

The expected reduction in improvement at q designs $\mathbf{x}'_{1:q}$ when adding new points $\mathbf{x}_{(N+1):(N+p)}$ is given by the general qERCI criterion:

$$\begin{aligned}
qERCI(\mathbf{x}'_{1:q}|\mathbf{x}_{(N+1):(N+p)}) &\triangleq \mathbb{E} \left[\left(T_N - \min_{i \in \{1, \dots, q\}} Y(\mathbf{x}'_i) \right)_+ \right] - & (10) \\
&\mathbb{E} \left[\left(T_N - \min_{i \in \{1, \dots, q\}} Y(\mathbf{x}'_i) | \mathbf{x}_{(N+1):(N+p)} \right)_+ \right] \\
&= qEI(\mathbb{E}[Y(\mathbf{x}'_{1:q})], \text{Cov}[Y(\mathbf{x}'_{1:q})]) - & (11) \\
&qEI(\mathbb{E}[Y(\mathbf{x}'_{1:q})], \text{Cov}[Y(\mathbf{x}'_{1:q}) | \mathbf{x}_{(N+1):(N+p)}]).
\end{aligned}$$

The first part is the standard parallel expected improvement (qEI), based on $Y(\mathbf{x})$, while the second term is the parallel expected improvement for $Y(\mathbf{x})|\mathbf{x}_{(N+1):(N+p)}$. Fortunately, qEI also has a closed-form expression [15], and its gradient can be computed analytically [39], making evaluations relatively fast when q is small. For larger q , an efficient approximation is provided by [6].

In practice, $\mathbf{x}_{(N+1):(N+p)}$ are the points that will be tentatively evaluated, including replicates, while $\mathbf{x}'_{1:q} = (\mathbf{x}_c, \mathbf{x}_n^*, \mathbf{x}_{(n+1):(N+p)})$. The behavior of the qERCI criterion when adding a single new design is depicted in Figure 2. As can be seen, depending on the number of possible replicates and noise variance, the best location may be a replicate of already evaluated designs.

3.4 Joint selection of \mathbf{x}_{n+1} and a_{n+1}

For non-myopic infill criteria, additional replications always provide more information gain. Because evaluations are costly, however, controlling the replication budget a_{n+1} is essential in practice.

Rather than deciding a_{n+1} once \mathbf{x}_{n+1} is found, it can be decided beforehand based on a minimal variance reduction. Indeed, in a low signal-to-noise setting, a single observation typically has limited impact on the GP prediction. Consequently, we propose replicating enough to achieve a predefined reduction in the predictive variance. That is, let this adaptive number of replicates $p_a(\mathbf{x})$ be the fewest number of replications p at $\mathbf{x}_{n+1} = \mathbf{x}$ such that $\frac{s_n^2(\mathbf{x}) - s_{n+1}^2(\mathbf{x})}{s_n^2(\mathbf{x})} \geq T_a$, where T_a is a user-specified threshold (e.g., $T_a = 0.2$). From (9),

$$p_a(\mathbf{x}) = \lceil r^2(\mathbf{x}_{n+1})(s_n^2(\mathbf{x}, \mathbf{x})/T_a - s_n^2(\mathbf{x}, \mathbf{x})) \rceil. \quad (12)$$

Then the acquisition function is computed with $a_{n+1} = p_a$ replicates at \mathbf{x} , which we call version 1 of

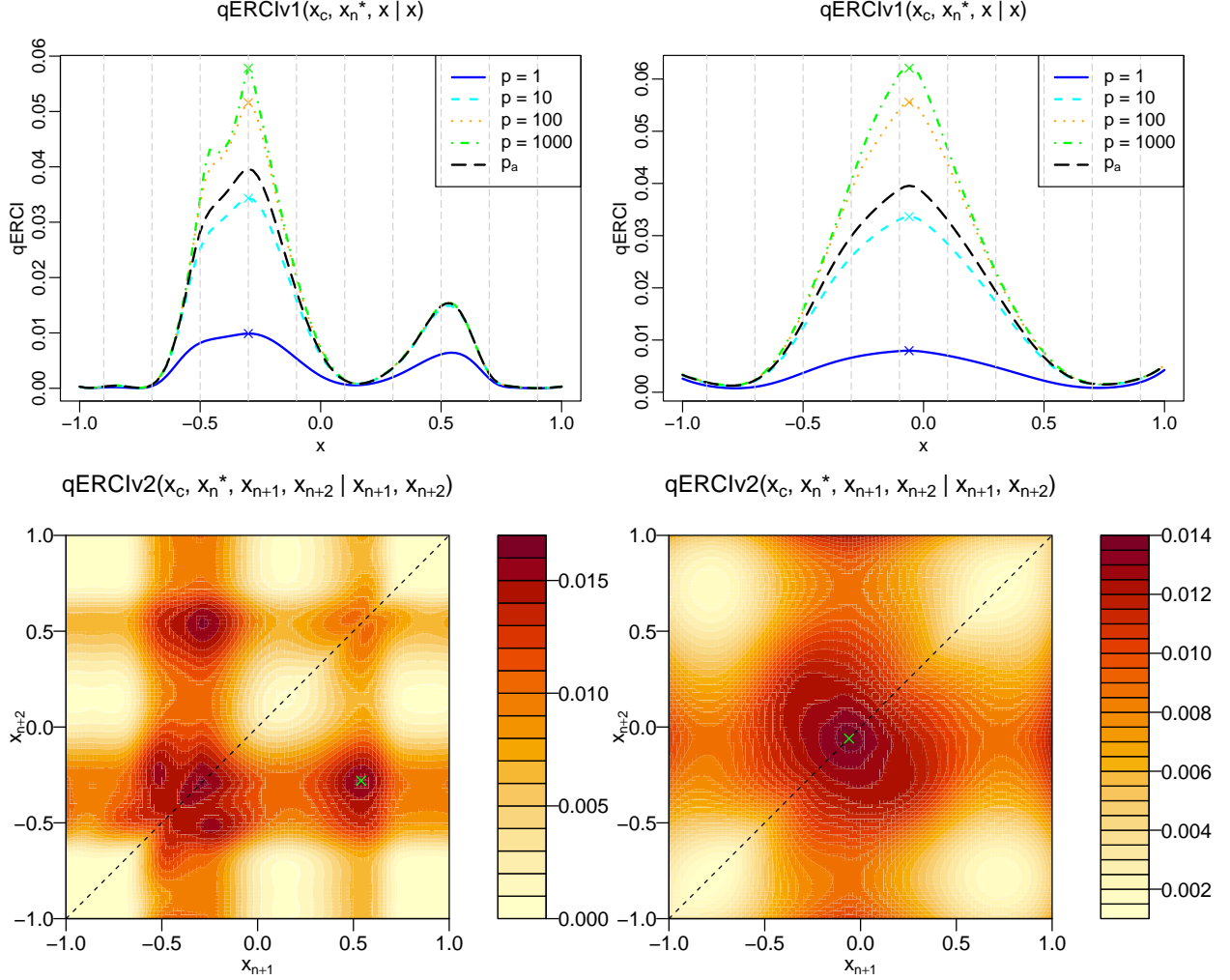


Figure 2: Parallel reduction in improvement example for the cases in Figure 1, one case per column. Crosses mark the respective maxima. Top: qERCI for one new point \mathbf{x}_{n+1} allowing for various numbers of replicates ($a_{n+1} = p$). Bottom: qERCI for two new points with a single replicate. The dashed line marks where $\mathbf{x}_{n+1} = \mathbf{x}_{n+2}$.

qERCI:

$$qERCIv1(\mathbf{x}) \triangleq qERCI \left((\mathbf{x}_c, \mathbf{x}_n^*, \mathbf{x}) \mid \left(\mathbf{x}, \overset{p_a(\mathbf{x}) \text{ times}}{\dots}, \mathbf{x} \right) \right). \quad (13)$$

This is illustrated in Figure 2. Compared with options with a fixed number of replicates, this adaptive version can suggest taking more or fewer replicates and does not follow a specific fixed p curve.

Next we focus on the case where there is a setup cost c_0 (say, meshing for finite element models, or an experimental setup) that needs to be paid only once for several replicates, each with a smaller cost of c_1 . The cost for p evaluations of a given \mathbf{x} is then $c_0 + pc_1$. The benefit of introducing a cost function is to balance with the increased value from replicating of look-ahead acquisition functions (that show the diminishing return property when adding new replicates). Thus, the cost must increase sufficiently to penalize adding too many replicates.

Introducing a second possible new design is another option to assess when to stop replicating. In this case it suffices to optimize qERCI with respect to $\mathbf{x}_{n+1}, a_{n+1}$ and $\mathbf{x}_{n+2}, a_{n+2}$, with up to $a_{n+1} + a_{n+2} \leq p_{\max}$ replicates. By dividing by the setup costs, it should naturally limit the number of replicates; and with $c_0 > 0$, the interest of a second new point may be diminished if not bringing enough gain compared to replicates on the first one. This is the second version of qERCI that we propose:

$$qERCIv2(\mathbf{x}, a, \mathbf{x}', a', c_0, c_1) \triangleq \frac{qERCI\left(\left(\mathbf{x}_c, \mathbf{x}_n^*, \mathbf{x}, \mathbf{x}'\right) \mid \left(\mathbf{x}, \overset{a \text{ times}}{\dots}, \mathbf{x}, \mathbf{x}', \overset{a' \text{ times}}{\dots}, \mathbf{x}'\right)\right)}{c_0 \times (\mathbf{1}_{a>0} + \mathbf{1}_{a'>0}) + c_1 \times (a + a')}. \quad (14)$$

The replication budget may be optimized as a continuous variable for simplicity: Eq. (9) does not need an integer valued p but ultimately it must be rounded for the evaluation. If splitting the replication budget between two candidates is preferred ($a_{n+1} > 0$ and $a_{n+2} > 0$), the one with the largest number of replicates is evaluated.

We entertain this strategy on the previous examples, optimizing $qERCIv2$ over x, x', a, a' by running a particle swarm optimization for global search, before applying L-BFGS-B to the best candidate. Depending on the cost function, as seen in Tables 1 and 2, all the evaluation budget is used or split between two candidates, or not.

Table 1: Results for the left case in Figure 2. The maximum number of replicates is $p_{\max} = 10$. For zero costs, the value of the denominator in $qERCIv2$ is set to 1.

c_0	c_1	x_{n+1}	a_{n+1}	x_{n+2}	a_{n+2}	qERCIv2
0	0	-0.29	7	0.54	3	0.041
1	1	-0.29	2	-	-	0.016
1	0.1	-0.29	6	-	-	0.028
1	0.001	-0.29	10	-	-	0.034

Table 2: Results for the right case in Figure 2. The maximum number of replicates is 10. For zero costs, the value of qERCI is divided by 1 in the search.

c_0	c_1	x_{n+1}	a_{n+1}	x_{n+2}	a_{n+2}	qERCIv2
0	0	-0.061	9	1	1	0.036
1	1	-0.061	2	-	-	0.014
1	0.1	-0.059	8	-	-	0.031
1	0.001	-0.059	10	-	-	0.034

4 Adaptations for TR-Based Bayesian Optimization

Although trust-region-based BO methods have shown promise in the deterministic case, several important considerations arise when adapting them to the low signal-to-noise ratio regime.

4.1 Handling of non-stationarity and replication

To address non-stationarity in the objective function, one can adopt non-stationary covariance kernels [48], pseudo-inputs [61], or local models [26]. We choose local models because they also reduce computational

cost and naturally pair with the TR framework, which restricts attention to observations within the current trust region rather than the entire domain.

In practice, we scale inputs in the trust region to $[-1, 1]^d$ and scale outputs by subtracting their mean and scaling by their standard deviation, which avoids numerical difficulties with very small or large output values and simplifies the setting of hyperparameter bounds. We then apply simple kriging (i.e., assuming a known constant mean of zero).

For replication, we rely on the approach of [9] to leverage the associated computational savings. This method can also either estimate a constant noise level or learn an input-dependent noise GP for $r^2(\mathbf{x})$ by a joint likelihood approach on the mean and variance GP processes. The stochastic kriging [2] approach could be used as well, but it requires a second GP fitted on empirical variance estimates to predict the variance at arbitrary locations (hence a minimal degree of replication). When the noise variance depends on the input, learning it is beneficial, but it also comes with additional inference and computational complexity. Moreover, when the noise variance is smooth and the TR radius decreases, the benefit of modeling heteroscedasticity becomes less important. Consequently, unless the noise is assumed to be constant, we allow the heteroscedastic model to revert to an homoscedastic one as proposed by [7], based on the comparison between their likelihoods. In both cases, the model is trained on the n_b closest points to the TR center. This helps improve the local accuracy of the model and further reduce computational costs.

4.2 Acceptance test

From the benchmarking study in [30], it is identified that accurately ranking and selecting the “best” evaluated point is crucial. In a trust-region setting, this task is simpler: we need to determine only whether the new candidate outperforms the current center.

A key quantity governing the TR method for deterministic objectives is the acceptance ratio: $\rho_n = \frac{f(\mathbf{x}_c) - f(\mathbf{x}_{n+1})}{m_n(\mathbf{x}_c) - m_n(\mathbf{x}_{n+1})}$. When noise is present, using the noisy function values is not reasonable, but their updated model values could be used instead: $m_{n+1}(\mathbf{x}_c)$ and $m_{n+1}(\mathbf{x}_{n+1})$. Then we can actually compute the acceptance ratio, although the numerator and denominator of ρ_n are no longer independent quantities.

In our framework we also compute the denominator in the acceptance ratio using leave-one-out predictions under the same (updated) GP model used for the numerator—in other words, the updated GP model after observing the data at \mathbf{x}_{n+1} . The leave-one-out predictions at \mathbf{x}_i , that is, after removing the corresponding observation, have closed-form expressions [4, 19]:

$$\tilde{m}_n(\mathbf{x}_i) = \bar{y}_i - [(\mathbf{K}_n + \mathbf{\Lambda}_n \mathbf{A}_n^{-1})^{-1} \bar{\mathbf{y}}]_i / [(\mathbf{K}_n + \mathbf{\Lambda}_n \mathbf{A}_n^{-1})^{-1}]_{i,i}, \quad (15)$$

$$\tilde{s}_n^2(\mathbf{x}_i) = [(\mathbf{K}_n + \mathbf{\Lambda}_n \mathbf{A}_n^{-1})^{-1}]_{i,i} - r^2(\mathbf{x}_i) / a_i. \quad (16)$$

This approach differs from simply relying on the previous GP model in that the covariance hyperparameters can be more precisely estimated with the additional data at the newly sampled design.

To decide on the next center, the decision is generally based on the value of the mean. To make this step more robust, we add a constraint on the relative variance between $Y(\mathbf{x}_c)$ and $Y(\mathbf{x}_{n+1})$. Indeed, a deceptive case can occur when the variance at $Y(\mathbf{x}_{n+1})$ is large and the corresponding mean is lower than for $Y(\mathbf{x}_c)$, while this can simply be an overoptimistic estimate due to the noise variance. To prevent this case, the number of replicates a_{n+1} at \mathbf{x}_{n+1} is increased such that $\mathbb{V}[Y(\mathbf{x}_{n+1})] \leq 4\mathbb{V}[Y(\mathbf{x}_c)]$. If this inequality is not

satisfied after updating with the observations, the new point cannot be accepted as the center until more data is available.

Another corner case that may occur is when the new point selected by the acquisition function leads to a predicted decrease that is negative (i.e., corresponding to exploration, with large predictive variance). There the acceptance ratio should be computed differently: $\rho_n = \frac{m_{n+1}(\mathbf{x}_c) - m_{n+1}(\mathbf{x}_{n+1}) - (\tilde{m}_{n+1}(\mathbf{x}_c) - \tilde{m}_{n+1}(\mathbf{x}_{n+1}))}{|\tilde{m}_{n+1}(\mathbf{x}_{n+1}) - \tilde{m}_{n+1}(\mathbf{x}_c)|}$. This modification accommodates *good surprises* by allowing for the possibility that the actual observed improvement might exceed the model’s initial negative prediction.

4.3 Reducing the trust-region radius

As trust-region methods progress, they must decrease the TR radius in order to improve model quality and find continued decrease. In noisy settings, however, this can be problematic: as the radius shrinks by a coefficient γ_{dec} , the local signal-to-noise ratio also declines, causing the predictive surface to become flatter and more uncertain. This, in turn, makes identifying points where the function is improved increasingly difficult, which can then trigger further radius reductions and exacerbate the issue. In such cases, the TR radius should *not* be decreased.

To identify when this situation arises, we compare the contributions to the variance of y over the TR domain Ω , that is, $\mathbb{V}[y(X)|X \sim \mathcal{U}(\Omega)]$. For a GP model Y , the law of total variance gives

$$\mathbb{E}[Y] = \mathbb{E}[\mathbb{E}[Y|X]] = \mathbb{E}[m_n(X)], \quad (17)$$

$$\mathbb{V}[Y] = \mathbb{E}[\mathbb{V}[Y|X]] + \mathbb{V}[\mathbb{E}[Y|X]] = \mathbb{E}[s_n^2(X)] + \mathbb{V}[m_n(X)]. \quad (18)$$

For $\mathbb{V}[Y]$, the first term is the integrated mean squared prediction error (IMSE), and the second term can be written as

$$\mathbb{V}[m_n(X)] = \mathbb{E}[m_n(X)^2] - \mathbb{E}[m_n(X)]^2 = (\mathbf{K}_n^{-1}\mathbf{y})^\top \mathbb{V}[k(X, \mathbf{x}_{1:n})] (\mathbf{K}_n^{-1}\mathbf{y}).$$

Both have known expressions for the standard Gaussian or Matérn kernels; see, for example, [10]. We illustrate the idea in [Figure 3](#). On the left, the leading contribution is the variance of the mean, while on the right it is the predictive variance. In this case, reducing the TR radius would be detrimental.

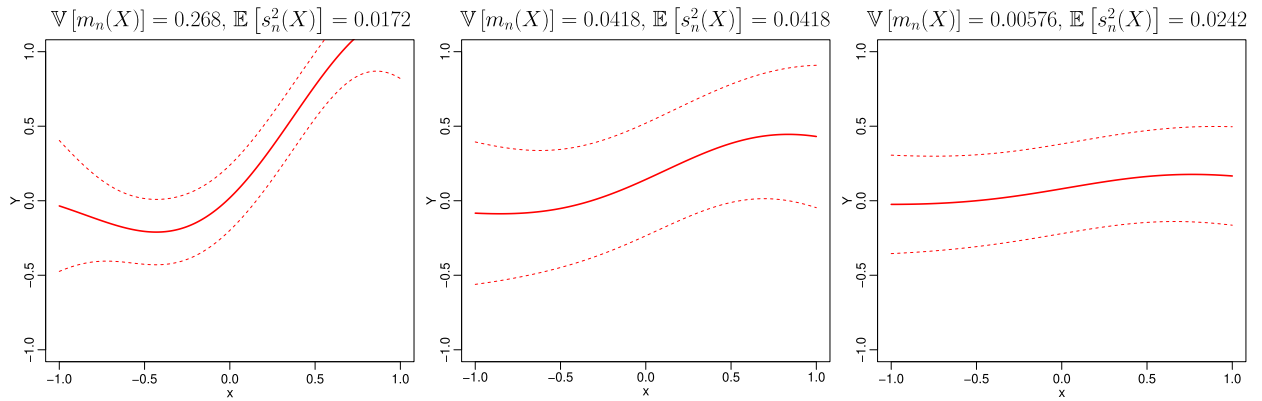


Figure 3: Gaussian processes with various variance of the mean vs. mean predictive variance ratios.

4.4 Summary of the approach

These elements are generic and may be integrated within existing TR frameworks. Next we detail one instantiation.

The full GP-based TR algorithm pseudocode is summarized in [Algorithm 1](#). A GP prior can be defined with an arbitrary number of initial points (even no points). In practice, Step 2 uses an initial design of experiments consisting of a Latin hypercube sample (LHS) of size $N_0 = \min(10, 2d)$, selected according to the maximin criterion. No replicates are needed at this stage. While N appears to represent the current number of observations, the actual number of iterations depends on the number of unique designs n . The initial TR center \mathbf{x}^0 can be provided; otherwise, it corresponds to the initial design point with the best predictive mean. In Step 6, if the number of designs in the TR is too small, new points are added while enforcing a minimal variance reduction based on the latest GP model (either the initial one from Step 2 or one built on the n_b closest points to the TR center in Step 8). These new designs are uniformly sampled in the TR region, which has been shown to help learning the GP hyperparameters by [\[69\]](#). As in TRIKE [\[57\]](#) or ORBIT [\[67\]](#), the minimal number of designs is set to $d + 1$. For computational speed, in Steps 8 and 13 it is possible to relearn the GP hyperparameters only every few iterations, following a fixed schedule as in [\[38\]](#).

In Step 9, the acquisition function is optimized over the TR. In our implementation, it starts from a uniformly sampled set of candidates of size $\min(100d, 5000)$ before performing local optimization with L-BFGS-B starting from the best candidate. For EI, since it does not take the replication effort into account, a_{n+1} is simply determined based on the minimal variance reduction T_a . For qERCIV2, which involves more variables to optimize, the initial uniform sample is replaced by a particle swarm optimization with 50 particles over 40 iterations. As discussed in [Section 4.2](#), Step 10 imposes that the future predictive variance at the new point is not too large in order to stabilize the update of the TR center; a_{n+1} may be increased accordingly in Step 11, before evaluating the new design with a_{n+1} replicates (Step 12). The GP model is then updated in Step 13 to estimate whether the progress brought by the new point is sufficient (Step 14). If so, the acceptance ratio ρ_n is computed (Step 15) based on the predictive mean and its LOO version (see [Section 4.2](#)). If the ratio is sufficiently large, the TR radius is increased (Step 17); otherwise, the TR radius may be decreased (Step 19) depending on the estimated signal-to-noise ratio (see [Section 4.3](#)). The same condition is checked if the iteration was unsuccessful (Step 22). This handling of the TR radius is closer in spirit to TRIKE [\[57\]](#) than to TurBO [\[20\]](#), where the number of consecutive successes or failures triggers TR radius changes.

The effect of the various parameters of the approach (γ_{dec}, T_a , the future predictive variance threshold in Step 10, or the IMSE criterion in Step 22) is studied in [Appendix A](#). Summarizing the results, γ_{dec} has little influence compared to the IMSE parameter. In particular, reducing the IMSE constant, which makes the TR reduction criterion less strict, degrades performance. The effect of the minimal variance reduction T_a shows that it is not necessary to reduce it too aggressively, e.g., by 50%. The same conclusion applies to the variance ratio between the TR center and the new design: a reduction that is too large is detrimental, while reducing it excessively also starts degrading performance. The remaining parameter values (β, η) take acceptable values from the literature.

Algorithm 1: Pseudocode for GP-based TR method

Require: $0 < \gamma_{\text{dec}}(0.8) < 1 < \gamma_{\text{inc}}(1/\gamma_{\text{dec}})$, $0 < \eta(0.2)$, $\beta(10^{-3}) < 1$, n_b (number of neighbors), N_0 ($2 \times d$, initial number of observations), acquisition function α , N_{max} (budget), p_{max} (max number of replication), \mathbf{x}^0 (initial TR center), $0 < \Delta_0$ (initial TR radius), T_a (0.2, minimal variance reduction).

Set $\mathbf{x}_c = \mathbf{x}^0$, $\Delta = \Delta_0$;

Construct initial design of experiments: e.g., maximin LHS of size N_0 ;

$N = N_0$;

Build initial GP model;

while $N \leq N_{\text{max}}$ and $\Delta > \Delta_{\text{min}}$ **do**

if Number of points in the TR $< d + 1$ **then**

 | Augment the DoE to have $d + 1$ points;

end

 Update GP model Y_N (mean m_n , variance s_n^2) conditioned on the n_b nearest neighbors of \mathbf{x}_c (normalize inputs in the TR, normalize outputs);

 Compute \mathbf{s} , $a_{n+1} \in \arg \max_{\mathbf{s}: \|\mathbf{s}\| \leq \Delta, p \leq p_{\text{max}}} \alpha(\mathbf{x}_c + \mathbf{s})$;

if $s_{n+1}^2(\mathbf{x}_c + \mathbf{s}) > 4s_n^2(\mathbf{x}_c)$ **then**

 | Increase a_{n+1} (up to p_{max}) based on (12);

end

 Evaluate $f(\mathbf{x}_c + \mathbf{s})$ with replication number a_{n+1} ;

 Update GP: $Y_{N+a_{n+1}}$: m_{n+1} , s_{n+1}^2 ;

if $m_{n+1}(\mathbf{x}_c) - m_{n+1}(\mathbf{x}_c + \mathbf{s}) \geq \beta \min \{ \Delta, \Delta^2 \}$ **then**

 | Calculate $\rho_n = \frac{m_{n+1}(\mathbf{x}_c) - m_{n+1}(\mathbf{x}_c + \mathbf{s})}{\tilde{m}_{n+1}(\mathbf{x}_c) - \tilde{m}_{n+1}(\mathbf{x}_c + \mathbf{s})}$;

if $\rho_n \geq \eta$ and $s_{n+1}^2(\mathbf{x}_c + \mathbf{s}) \leq 4s_n^2(\mathbf{x}_c)$ **then**

 | $\mathbf{x}_c = \mathbf{x}_c + \mathbf{s}$; $\Delta = \gamma_{\text{inc}}\Delta$;

else

if $\mathbb{V}[m_n(X)] \geq 10\mathbb{E}[s_n^2(X)]$ **then**

 | $\Delta = \gamma_{\text{dec}}\Delta$;

end

end

end

else

if $\mathbb{V}[m_n(X)] \geq 10\mathbb{E}[s_n^2(X)]$ **then**

 | $\Delta = \gamma_{\text{dec}}\Delta$;

end

end

end

$N = N + a_{n+1}$;

Return \mathbf{x}_c and estimated value $m_n(\mathbf{x}_c)$

5 Empirical evaluation

We now compare the capabilities of the proposed GP-based TR method for stochastic optimization, dubbed OGPIT for optimization by Gaussian processes in trust regions. In a first phase we test the ability to reach a local optimum efficiently; then we evaluate the proposed cost-aware version.

We focus on local optimization to avoid confusion coming from the global optimization level. Also, issues with existing methods become preponderant when the signal-to-noise ratio decreases, as happens when the trust-region radius becomes small. We consider two sets of benchmark functions. Benchmark 1 includes simple validation test functions plus a typical function from the BO literature (i.e., Branin): sphere function (2d, 4d, 6d), squared sphere function (2d, 4d, 6d), Branin (2d), and Rosenbrock (2d, 4d). Benchmark 2 is obtained from the BendFO repository [34, 44], which consists of nonlinear least squares problems of the form $\sum_{i=1}^m f_i(\mathbf{x})^2$. We restrict the analysis to the smooth problem type and instances of dimension lower than 10, resulting in 36 different test problems.

As baselines, we compare with the state-of-the-art GP-based trust-region optimizer TuRBO [20] and regular BO from the BoTorch Python library [5]. We remark that TuRBO, while it can run on stochastic problems, is initially dedicated for deterministic problems and thus is not expected to find precise solutions. BoTorch is a global optimization method, hence not necessarily suited for precise convergence on local optimization problems. Closer to polynomial-surrogate-based TR methods, we also run SNOWPAC on Benchmark 1, as it also relies on a GP model. Since these methods do not exploit replication, the computational cost increases quickly with N . To keep reasonable timings, we enforce a 10-minute stopping time, which is too small for SNOWPAC on Benchmark 2.

TuRBO relies on the Thompson sampling acquisition function, BoTorch and OGPIT on EI, while SNOWPAC optimizes the mean prediction directly. TuRBO, BoTorch and SNOWPAC evaluate only a single new point without replicate at each iteration, while OGPIT uses p_a replicates (and $p_{\max} = 500$).

We let each method use its own initial design procedure, but with the same number of initial designs. For SNOWPAC, we provide a starting solution. For Benchmark 2, as it contains starting points, these are also passed to all methods.

We entertain versions of the test functions with no noise for validation, then with zero mean Gaussian additive noise with standard deviation equal to 0.001, 0.01, and 0.1 (resp. 0.001, 0.1, and 10) for Benchmark 1 (resp. 2). We compute the regret over iterations, that is, the difference to the reference solution. For OGPIT, the regret is computed on the trust-region center value. For BoTorch, SNOWPAC and TuRBO, it is computed on all evaluated points, hence favoring these methods. The results are summarized through data profiles of the regret. For a given amount of evaluations, a data profile shows the proportion of problems solved for a given precision, based on the best solution found among the considered methods. Data profiles are detailed in [44]. Results are normalized by $d + 1$ to compare problems of various dimensions.

Each test problem is repeated 30 times since results depend on the initial designs or starting point. Two versions of the code, one in R and one in Python, are available here: <https://github.com/POptUS/StochDFO>.

5.1 Local optimization without setup cost

We use a maximum budget of $N_{\max} = 10^4(d + 1)$. The performance is compared first on Benchmark 1, with results provided in Figure 4. For noiseless problems, OGPIT and TuRBO perform similarly for the

highest gates, but OGPIT and SNOWPAC outperforms on the smaller ones. BoTorch underperforms for all cases, failing to converge precisely on these simple problems (only $\sim 60\%$ of problems solved even for the largest gate). As the noise variance increases, the performance of TuRBO degrades compared with OGPIT, especially for the smallest gates. SNOWPAC shows the best results in the early stages, helped by its quadratic surrogate on these convex test problems. As the noise increases, the performance degrades compared to OGPIT. Then, as it cannot scale to larger number of iterations, its performance plateaus.

We illustrate the outcome of the adaptive replication strategy in [Appendix B](#), where we show in [Figure 13](#) how the number of replication evolves over iterations for OGPIT. It depends both on the problem instance and its dimension, which makes fixing a replication number a priori difficult. Indeed, fixing the replication effort in OGPIT degrades the performance, see [Figure 14](#).

Next we provide results for the more complex Benchmark 2 in [Figure 5](#). Again, OGPIT outperforms TuRBO, with larger gaps with increasing noise. The results show the effect of the lower signal-to-noise ratio as the TR radius reduces. Here BoTorch performs poorly for all cases, even the noiseless one, because of the bad conditioning close to the solution and because of the large difference in objective values observed in single problems in this benchmark set. This is generally difficult for surrogate models. Local models are more suited in this context. For the first iterations, most methods perform similarly. Then TuRBO and BoTorch tend to stagnate while OGPIT keeps improving.

5.2 Local optimization with setup cost

For emulating the behavior with our motivating setup cost structure, we ran OGPIT on Benchmark 1 and present average results over costs. We use a maximum cost of 1000, with $c_0 = 1$ and $c_1 = 10^{-4}, 10^{-3}, 10^{-2}$.

As the default method, as in the preceding section we use EI as the acquisition function. We then compare with the two variants of qERCI introduced in [Section 3.4](#). First this is OGPIT with qERCI v1, based on the adaptive strategy using p_a ($T_a = 0.2$) and dividing by the setup and replication cost. The number of replicates is such that the variance reduction at the new design is at least 20%.

The second method, dedicated for this setup cost is the qERCI v2 acquisition function. There OGPIT is with qERCI optimized over \mathbf{x}_{n+1} and \mathbf{x}_{n+2} . It entertains adding up to two new points with replicates based on the reduction in improvement divided by the cost. This emulates looking ahead by a batch strategy. Then only the design with the largest number of replicates is actually evaluated.

The results are provided in [Figure 6](#). For the smallest replication cost c_1 , the cost-aware version (qERCIv2) gives the best results with a large margin. For the medium replication cost scenario, it still outperforms the others. When the replication cost increases, it becomes equivalent to the default. The naive strategy of reducing the variance by 20% performs worse than the default acquisition function for all cost setups. Looking ahead further is thus preferable. The noise variance does not modify the ranking of the methods; it just translates the curves. Indeed, more evaluations are needed to reach a given regret level.

5.3 Motivating quantum test case

We consider a stochastic optimization problem arising from the quantum approximate optimization algorithm (QAOA) [\[21\]](#). QAOA is a prominent variational quantum algorithm and a candidate for demonstrating quantum advantage due to its relatively modest requirements on qubit counts and circuit depth compared

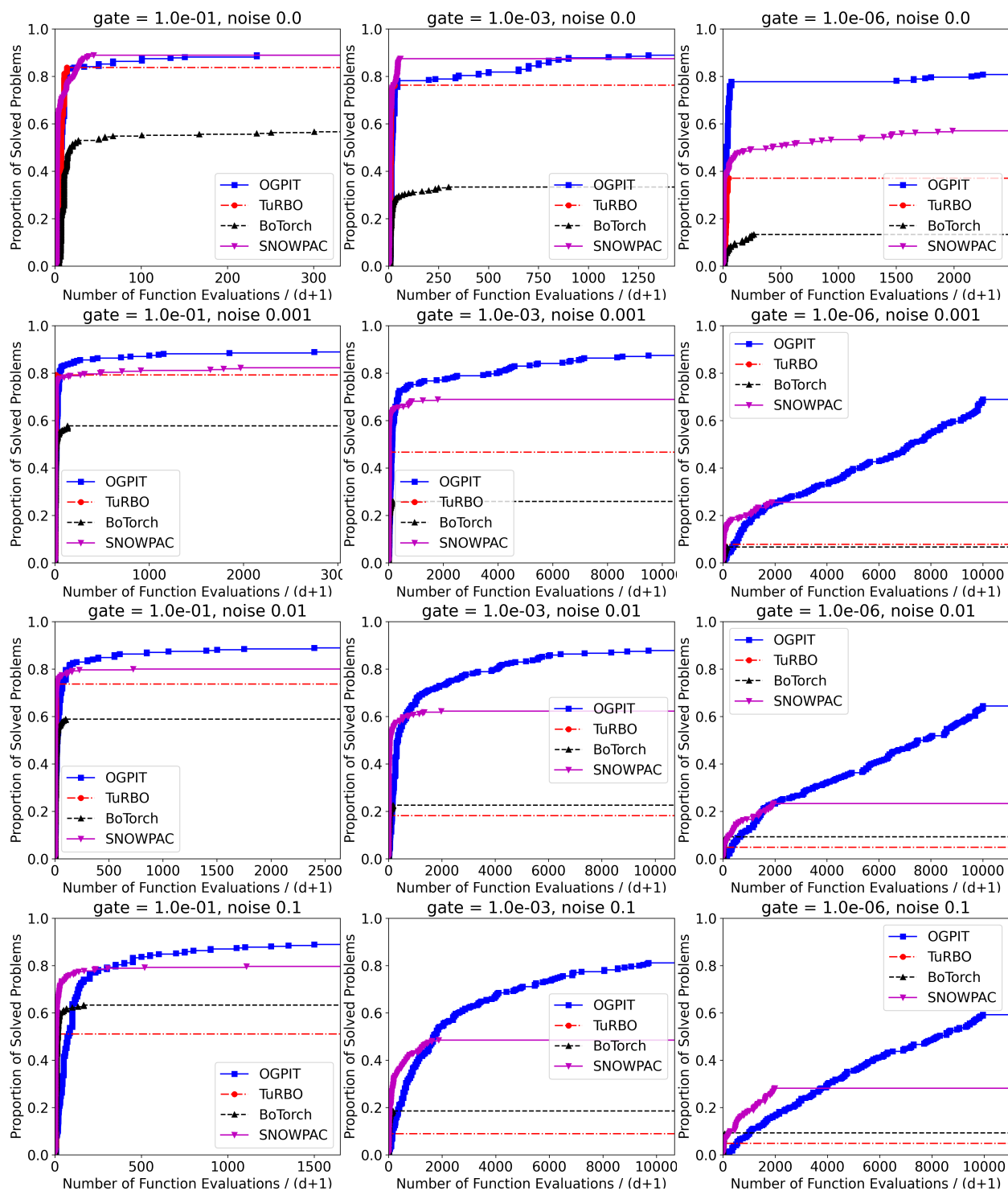


Figure 4: Data profiles of the method against TuRBO, SNOWPAC and BoTorch on Benchmark 1.

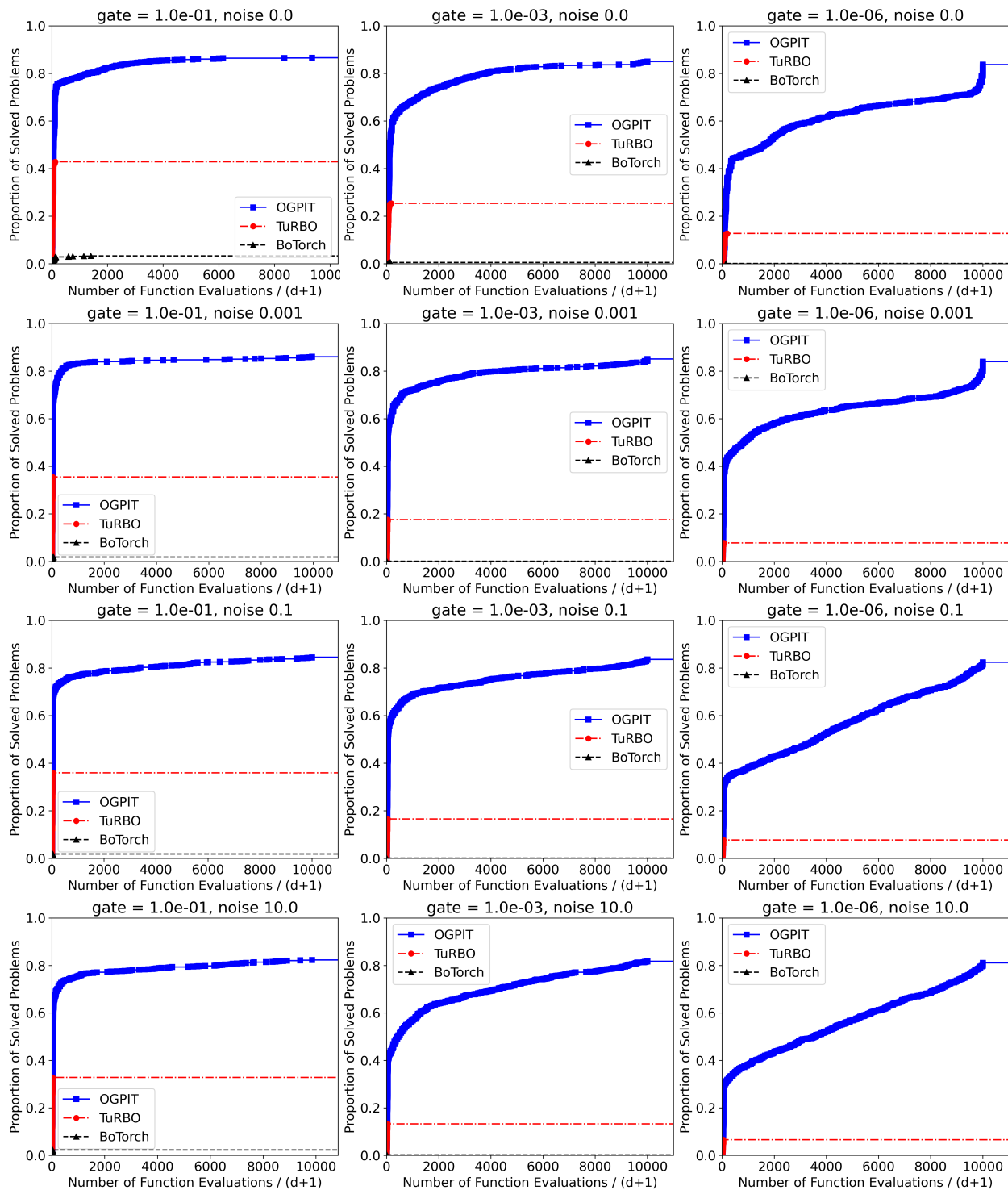


Figure 5: Data profiles of the method against TuRBO and BoTorch on Benchmark 2.

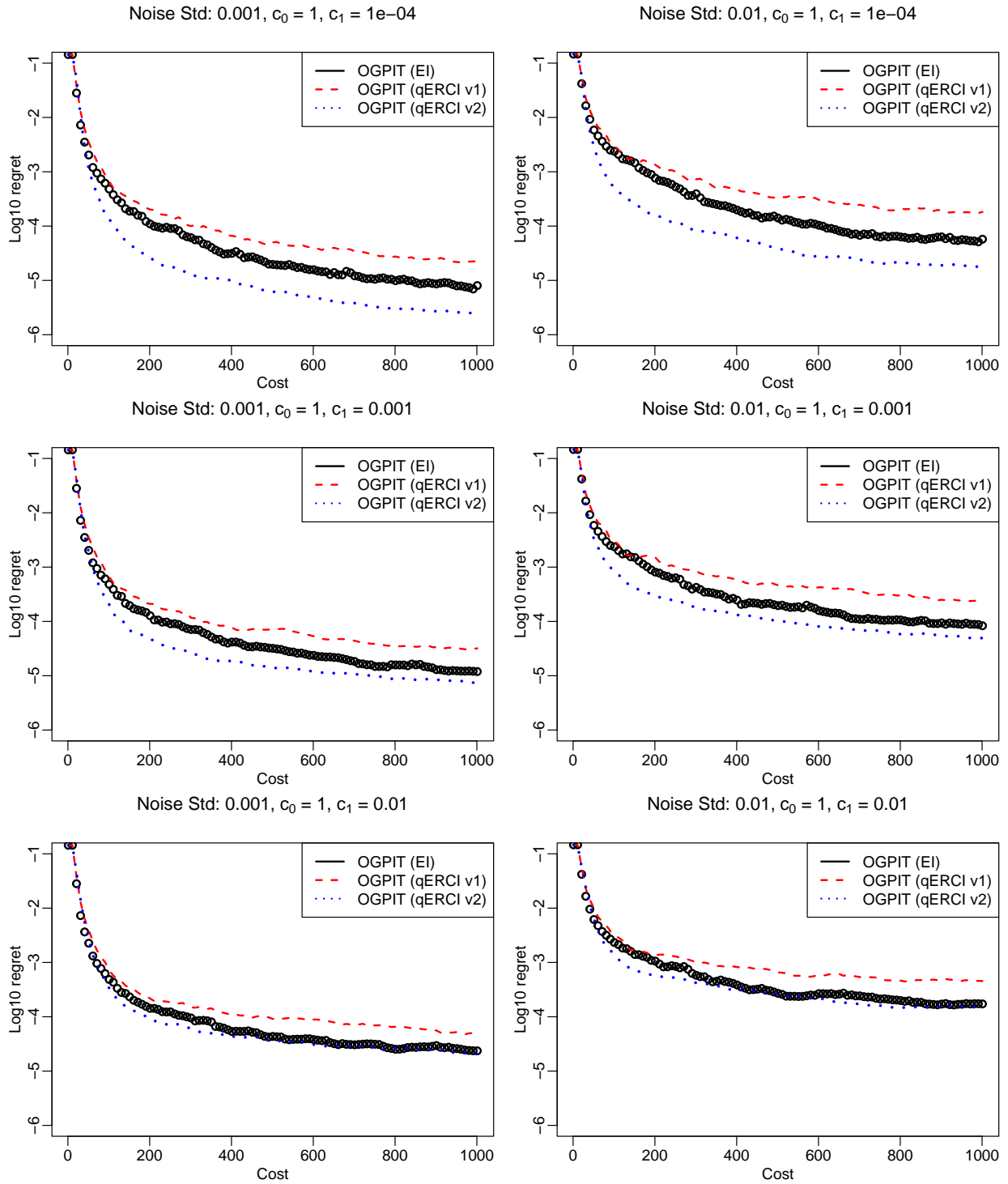


Figure 6: Results on Benchmark 1 with two noise levels and varying setup costs.

with fully fault-tolerant approaches [14, 53]. We consider using QAOA to solve Max-Cut problem instances on a collection of graphs $G = (V, E)$. Given a QAOA depth p , the algorithm requires $2p$ continuous parameters, typically written as

$$\theta = (\gamma_1, \dots, \gamma_p, \beta_1, \dots, \beta_p),$$

which define alternating applications of a cost Hamiltonian derived from the Max-Cut objective and a mixing Hamiltonian. The resulting objective value corresponds to the expected Max-Cut energy obtained by measuring the final quantum state. Finding high-quality parameters is widely recognized as a key bottleneck in the practical performance of QAOA [12, 27, 70].

The graphs we consider include the Chvátal graph and Erdős–Rényi graphs of increasing size, and the default experiments use $p = 1$ or $p = 2$ (so $d = 2p = 2$ or $d = 4$ parameters) ranging from 0 to $\pi/2$, rescaled to $[0, 1]$. We benchmark our approach on this stochastic objective, where the expectation is estimated using a finite number of measurement shots. As with most near-term quantum algorithms, QAOA is fundamentally stochastic in practice due to measurement noise and finite sampling. For the modest graph sizes considered here, however, the exact expectation value can be computed deterministically via classical simulation; we use these true values solely for benchmarking and diagnostic purposes. Each noisy function call returns multiple stochastic realizations, and the scalar test function aggregates these by taking the sample mean. This yields an unbiased estimator of the expected objective.

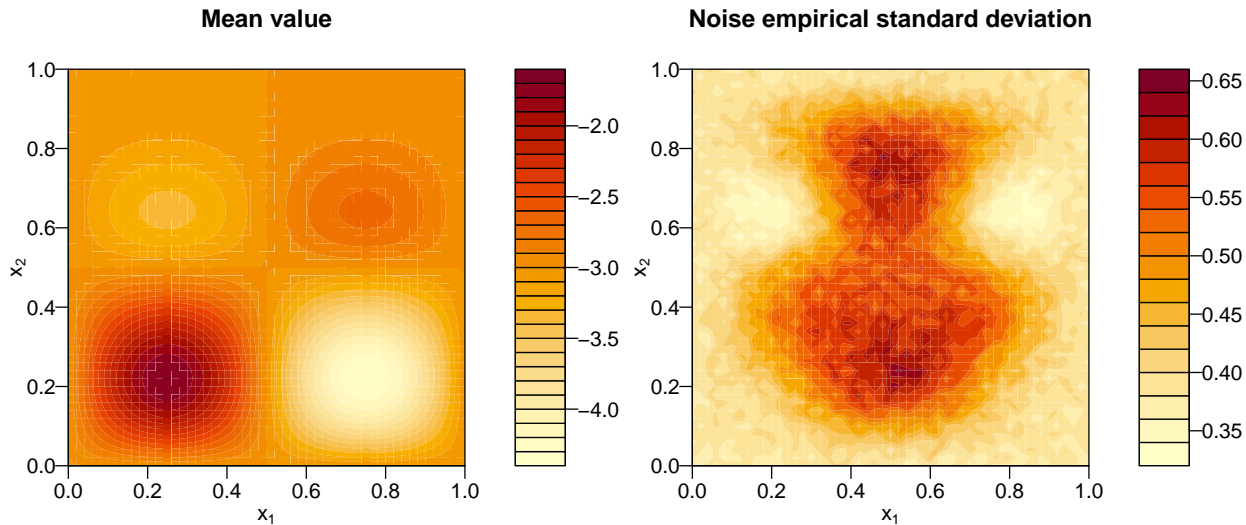


Figure 7: Illustration of the quantum test case with ground truth (left) and estimated noise standard deviation estimated over 5000 replicates.

This quantum test case exhibits several structural features that can be exploited by a trust-region Bayesian optimization framework. First, the noise variance is heteroscedastic (see Figure 7), varying significantly across the parameter domain due to the underlying quantum state amplitudes and measurement probabilities. Second, the problem is representative of settings with substantial setup costs: on average, preparing a circuit instance (i.e., configuring the parameterized quantum circuit and compiling it for execution) is approximately 100–1000 times more expensive than a single measurement shot. This cost structure arises because circuit preparation involves classical preprocessing, parameter loading, and potential compila-

tion or transpilation steps, whereas individual shots correspond only to repeated measurements of the same prepared circuit. We henceforth use $c_0 = 1$ and $c_1 = 0.001$ in our experiments, with a maximum cost of 250 for the $2d$ problem and 500 for the $4d$ problem. The initial design of experiments are of size 10 and 200, respectively, to ensure that the global optima are identified over the 5 repetitions of the experiment.

The results are presented in Figure 8, where the second version of qERCI again performs better at reducing the regret efficiently with respect to the cost. We note that the final regret is well below the noise variance.

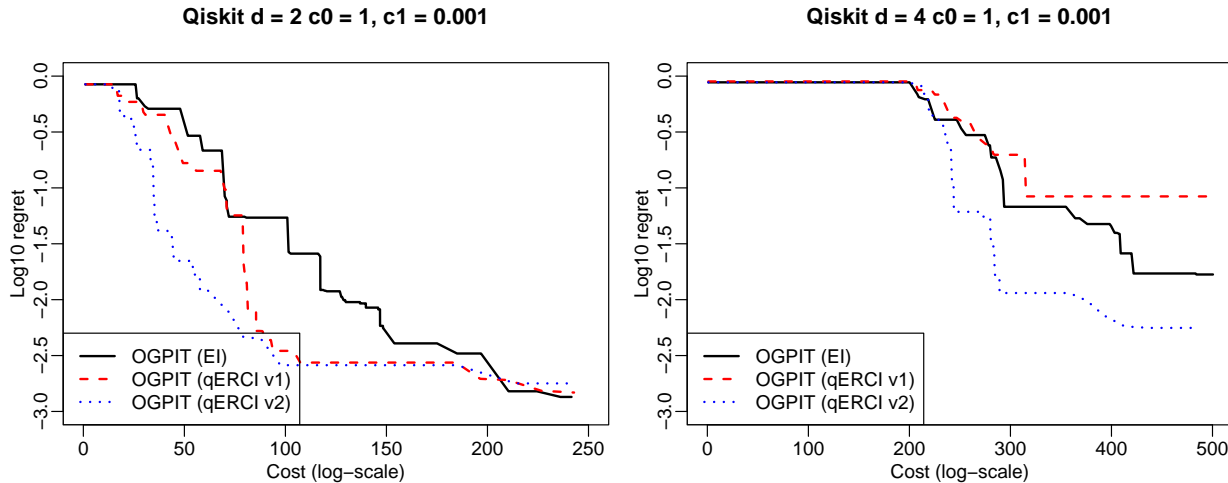


Figure 8: Results on the quantum test case, in dimension 2 (left) and dimension 4 (right).

6 Conclusion and perspectives

Standard Bayesian optimization provides efficient global optimization capabilities but is generally not well suited for precise convergence. For this purpose, trust-region-based Bayesian optimization strategies are more appropriate, and they perform well in benchmarks on noise-free problems; see, for instance, [59].

As we detail, the difficulty of current methods is exacerbated when noise is present. We therefore propose adaptations for noisy problems, including cases with large noise variance. In particular, selecting both the design to evaluate and the replication level allows us to control the accuracy of the model while maintaining computational scalability as the budget increases. Additional modifications to the trust-region mechanism are proposed, relying on properties of Gaussian processes. Targeting applications with significant setup costs but where repeating evaluations is comparatively inexpensive, we develop a dedicated acquisition function. We demonstrate the effectiveness of these modifications, showing good results even on noiseless test problems while yielding significant improvements when noise is present or when setup costs are substantial.

Although we focus on local optimization performance, possible future work includes studying the interplay with the global search phase of TR-based BO methods, since several options exist (e.g., [18, 20, 40, 41, 57]). Detecting when the function is unimodal in the trust region, as done in [42] but in the presence of noise, is a promising direction. Further work is also needed to study the effect of the input dimension when noise is present; high dimensionality is already a challenge even without noise and typically requires structural

assumptions; see, for example, [8].

Acknowledgments

This work was supported by the U.S. Department of Energy, Office of Science, Office of Advanced Scientific Computing Research, Scientific Discovery through Advanced Computing (SciDAC) Program through the FASTMath Institute under Contract No. DE-AC02-06CH11357. The authors are grateful to the OPAL infrastructure from Université Côte d’Azur for providing resources and support.

References

- [1] Mohamed Amine Bouhleb, Nathalie Bartoli, Rommel G Regis, Abdelkader Otsmane, and Joseph Morlier. Efficient global optimization for high-dimensional constrained problems by using the Kriging models combined with the partial least squares method. *Engineering Optimization*, 50(12):2038–2053, 2018. doi:[10.1080/0305215X.2017.1419344](https://doi.org/10.1080/0305215X.2017.1419344).
- [2] Bruce Ankenman, Barry L Nelson, and Jeremy Staum. Stochastic kriging for simulation metamodeling. *Operations Research*, 58(2):371–382, 2010. doi:[10.1287/opre.1090.0754](https://doi.org/10.1287/opre.1090.0754).
- [3] Charles Audet, Kwassi Joseph Dzahini, Michael Kokkolaras, and Sébastien Le Digabel. Stochastic mesh adaptive direct search for blackbox optimization using probabilistic estimates. *Computational Optimization and Applications*, 79(1):1–34, March 2021. ISSN 1573-2894. doi:[10.1007/s10589-020-00249-0](https://doi.org/10.1007/s10589-020-00249-0).
- [4] François Bachoc. Cross validation and maximum likelihood estimations of hyper-parameters of Gaussian processes with model misspecification. *Computational Statistics & Data Analysis*, 66:55–69, 2013. doi:[10.1016/j.csda.2013.03.016](https://doi.org/10.1016/j.csda.2013.03.016).
- [5] Maximilian Balandat, Brian Karrer, Daniel R. Jiang, Samuel Daulton, Benjamin Letham, Andrew Gordon Wilson, and Eytan Bakshy. BoTorch: A framework for efficient Monte-Carlo Bayesian optimization. In *Advances in Neural Information Processing Systems 33*, 2020. URL <https://proceedings.neurips.cc/paper/2020/file/f5b1b89d98b7286673128a5fb112cb9a-Paper.pdf>.
- [6] Mickaël Binois. *Uncertainty quantification on Pareto fronts and high-dimensional strategies in Bayesian optimization, with applications in multi-objective automotive design*. PhD thesis, Saint-Etienne, EMSE, 2015. URL <https://theses.hal.science/tel-01310521/>.
- [7] Mickael Binois and Robert B Gramacy. hetGP: Heteroskedastic Gaussian process modeling and sequential design in R. *Journal of Statistical Software*, 98(13):1–44, 2021. doi:[10.18637/jss.v098.i13](https://doi.org/10.18637/jss.v098.i13).
- [8] Mickael Binois and Nathan Wycoff. A survey on high-dimensional Gaussian process modeling with application to Bayesian optimization. *ACM Transactions on Evolutionary Learning and Optimization*, 2(2):1–26, 2022. doi:[10.1145/3545611](https://doi.org/10.1145/3545611).

- [9] Mickael Binois, Robert B Gramacy, and Mike Ludkovski. Practical heteroscedastic Gaussian process modeling for large simulation experiments. *Journal of Computational and Graphical Statistics*, 27(4): 808–821, 2018. doi:[10.1080/10618600.2018.1458625](https://doi.org/10.1080/10618600.2018.1458625).
- [10] Mickaël Binois, Jiangeng Huang, Robert B Gramacy, and Mike Ludkovski. Replication or exploration? Sequential design for stochastic simulation experiments. *Technometrics*, 61(1):7–23, 2019. doi:[10.1080/00401706.2018.1469433](https://doi.org/10.1080/00401706.2018.1469433).
- [11] Mickael Binois, Nicholson Collier, and Jonathan Ozik. A portfolio approach to massively parallel Bayesian optimization. *Journal of Artificial Intelligence Research*, 82:137–167, 2025. doi:[10.1613/jair.1.16868](https://doi.org/10.1613/jair.1.16868).
- [12] Fernando G. S. L. Brandão, Michael J. Broughton, Edward Farhi, Sam Gutmann, and Hartmut Neven. For fixed control parameters the quantum approximate optimization algorithm’s objective function value concentrates for typical instances. *arXiv:1812.04170*, 2018. doi:[10.48550/arXiv:1812.04170](https://doi.org/10.48550/arXiv:1812.04170).
- [13] Jian Cao, Joseph Guinness, Marc G Genton, and Matthias Katzfuss. Scalable Gaussian-process regression and variable selection using Vecchia approximations. *Journal of Machine Learning Research*, 23 (348):1–30, 2022. URL <https://jmlr.org/beta/papers/v23/22-0204.html>.
- [14] M. Cerezo, Andrew Arrasmith, Ryan Babbush, Simon C. Benjamin, Suguru Endo, Keisuke Fujii, Jarrod R. McClean, Kosuke Mitarai, Xiao Yuan, Lukasz Cincio, and Patrick J. Coles. Variational quantum algorithms. *Nature Reviews Physics*, 3(9):625–644, August 2021. ISSN 2522-5820. doi:[10.1038/s42254-021-00348-9](https://doi.org/10.1038/s42254-021-00348-9). URL <http://dx.doi.org/10.1038/s42254-021-00348-9>.
- [15] Clément Chevalier and David Ginsbourger. Fast computation of the multi-points expected improvement with applications in batch selection. In *International Conference on Learning and Intelligent Optimization*, pages 59–69. Springer, 2013. doi:[10.1007/978-3-642-44973-4_7](https://doi.org/10.1007/978-3-642-44973-4_7).
- [16] Clément Chevalier, David Ginsbourger, and Xavier Emery. Corrected kriging update formulae for batch-sequential data assimilation. In *Mathematics of Planet Earth: Proceedings of the 15th Annual Conference of the International Association for Mathematical Geosciences*, pages 119–122. Springer, 2013. doi:[10.1007/978-3-642-32408-6_29](https://doi.org/10.1007/978-3-642-32408-6_29).
- [17] Alexander I Cowen-Rivers, Wenlong Lyu, Rasul Tutunov, Zhi Wang, Antoine Grosnit, Ryan Rhys Griffiths, Alexandre Max Maraval, Hao Jianye, Jun Wang, Jan Peters, et al. HEBO: Pushing the limits of sample-efficient hyper-parameter optimisation. *Journal of Artificial Intelligence Research*, 74: 1269–1349, 2022. doi:[10.1613/jair.1.13643](https://doi.org/10.1613/jair.1.13643).
- [18] Youssef Diouane, Victor Picheny, Rodolphe Le Riche, and Alexandre Scotto Di Perrotolo. TREGO: A trust-region framework for efficient global optimization. *Journal of Global Optimization*, pages 1–23, 2022. doi:[10.1007/s10898-022-01245-w](https://doi.org/10.1007/s10898-022-01245-w).
- [19] Olivier Dubrule. Cross validation of kriging in a unique neighborhood. *Journal of the International Association for Mathematical Geology*, 15:687–699, 1983. doi:[10.1007/BF01033232](https://doi.org/10.1007/BF01033232).

- [20] David Eriksson, Michael Pearce, Jacob Gardner, Ryan D Turner, and Matthias Poloczek. Scalable global optimization via local Bayesian optimization. In *Advances in Neural Information Processing Systems*, pages 5497–5508, 2019. URL <https://dl.acm.org/doi/10.5555/3454287.3454780>.
- [21] Edward Farhi, Jeffrey Goldstone, and Sam Gutmann. A quantum approximate optimization algorithm. *arXiv:1411.4028*, 2014. doi:10.48550/arXiv:1411.4028.
- [22] Roman Garnett. *Bayesian Optimization*. Cambridge University Press, 2023. doi:10.1017/9781108348973.
- [23] David Ginsbourger and Rodolphe Le Riche. Towards Gaussian process-based optimization with finite time horizon. In *mODa 9—Advances in Model-Oriented Design and Analysis*, pages 89–96. Springer, 2010. doi:10.1007/978-3-7908-2410-0_12.
- [24] Javier González, Michael Osborne, and Neil D Lawrence. GLASSES: Relieving the myopia of Bayesian optimisation. In *Proceedings of the 19th International Conference on Artificial Intelligence and Statistics*, pages 790–799, 2016. URL <https://proceedings.mlr.press/v51/gonzalez16b.pdf>.
- [25] Robert B. Gramacy. *Surrogates: Gaussian Process Modeling, Design, and Optimization for the Applied Sciences*. Chapman and Hall/CRC, March 2020. doi:10.1201/9780367815493.
- [26] Robert B Gramacy and Daniel W Apley. Local Gaussian process approximation for large computer experiments. *Journal of Computational and Graphical Statistics*, 24(2):561–578, 2015. doi:10.1080/10618600.2014.914442.
- [27] Tianyi Hao, Zichang He, Ruslan Shaydulin, Jeffrey Larson, and Marco Pistoia. End-to-end protocol for high-quality quantum approximate optimization algorithm parameters with few shots. *Physical Review Research*, 7(3), August 2025. ISSN 2643-1564. doi:10.1103/24gg-7p8z. URL <http://dx.doi.org/10.1103/24gg-7p8z>.
- [28] James Hensman, Alexander G Matthews, Maurizio Filippone, and Zoubin Ghahramani. MCMC for variationally sparse Gaussian processes. *Advances in Neural Information Processing Systems*, 28, 2015. URL <https://dl.acm.org/doi/10.5555/2969239.2969423>.
- [29] Deng Huang, Theodore T Allen, William I Notz, and R Allen Miller. Sequential kriging optimization using multiple-fidelity evaluations. *Structural and Multidisciplinary Optimization*, 32:369–382, 2006. doi:10.1007/s00158-005-0587-0.
- [30] Hamed Jalali, Inneke Van Nieuwenhuyse, and Victor Picheny. Comparison of Kriging-based methods for simulation optimization with heterogeneous noise. *European Journal of Operational Research*, 261(1):279–301, 2017. doi:10.1016/j.ejor.2017.01.035.
- [31] Kirthevasan Kandasamy, Gautam Dasarathy, Jeff Schneider, and Barnabás Póczos. Multi-fidelity Bayesian optimisation with continuous approximations. In *International Conference on Machine Learning*, pages 1799–1808. PMLR, 2017. URL <https://proceedings.mlr.press/v70/kandasamy17a.html>.

- [32] Aaron Klein, Stefan Falkner, Simon Bartels, Philipp Hennig, and Frank Hutter. Fast Bayesian optimization of machine learning hyperparameters on large datasets. In *Artificial Intelligence and Statistics*, pages 528–536. PMLR, 2017. URL <https://proceedings.mlr.press/v54/klein17a.html>.
- [33] Jeffrey Larson and Stephen C. Billups. Stochastic derivative-free optimization using a trust region framework. *Computational Optimization and Applications*, 64(3):619–645, 2016. doi:10.1007/s10589-016-9827-z.
- [34] Jeffrey Larson and Stefan Wild. Benchmarking derivative-free optimization algorithms, 2025. URL <https://github.com/P0ptUS/BenDF0>. [Online; accessed 14-April-2025].
- [35] Jeffrey Larson, Matt Menickelly, and Stefan M Wild. Derivative-free optimization methods. *Acta Numerica*, 28:287–404, 2019. doi:10.1017/S0962492919000060.
- [36] Jeffrey Larson, Matt Menickelly, and Jiahao Shi. A novel noise-aware classical optimizer for variational quantum algorithms. *INFORMS Journal on Computing*, 37(1):63–85, 2025. doi:10.1287/ijoc.2024.0578.
- [37] Benjamin Letham, Brian Karrer, Guilherme Ottoni, and Eytan Bakshy. Constrained Bayesian Optimization with Noisy Experiments. *Bayesian Analysis*, 14(2):495 – 519, 2019. doi:10.1214/18-BA1110.
- [38] Xiong Lyu, Mickaël Binois, and Michael Ludkovski. Evaluating Gaussian process metamodels and sequential designs for noisy level set estimation. *Statistics and Computing*, 31(4):1–21, 2021. doi:10.1007/s11222-021-10014-w.
- [39] Sébastien Marmin, Clément Chevalier, and David Ginsbourger. Differentiating the multipoint expected improvement for optimal batch design. In *International Workshop on Machine Learning, Optimization and Big Data*, pages 37–48. Springer, 2015. doi:10.1007/978-3-319-27926-8_4.
- [40] Logan Mathesen, Giulia Pedrielli, and Szu Hui Ng. Trust region based stochastic optimization with adaptive restart: A family of global optimization algorithms. In *2017 Winter Simulation Conference (WSC)*, pages 2104–2115. IEEE, December 2017. doi:10.1109/wsc.2017.8247943. URL <http://dx.doi.org/10.1109/WSC.2017.8247943>.
- [41] Logan Mathesen, Giulia Pedrielli, Szu Hui Ng, and Zeld B Zabinsky. Stochastic optimization with adaptive restart: A framework for integrated local and global learning. *Journal of Global Optimization*, 79(1):87–110, 2021.
- [42] Mark McLeod, Stephen Roberts, and Michael A Osborne. Optimization, fast and slow: Optimally switching between local and Bayesian optimization. In *International Conference on Machine Learning*, pages 3443–3452. PMLR, 2018. URL <https://proceedings.mlr.press/v80/mcleod18a.html>.
- [43] Friedrich Menhorn, Florian Augustin, H-J Bungartz, and Youssef M Marzouk. A trust-region method for derivative-free nonlinear constrained stochastic optimization. *arXiv:1703.04156*, 2017. doi:10.48550/arXiv.1703.04156.
- [44] Jorge J Moré and Stefan M Wild. Benchmarking derivative-free optimization algorithms. *SIAM Journal on Optimization*, 20(1):172–191, 2009. doi:<https://doi.org/10.1137/080724083>.

- [45] Henry B Moss, Sebastian W Ober, and Victor Picheny. Inducing point allocation for sparse Gaussian processes in high-throughput Bayesian optimisation. In *International Conference on Artificial Intelligence and Statistics*, pages 5213–5230. PMLR, 2023.
- [46] Juliane Müller, Wim Lavrijsen, Costin Iancu, and Wibe de Jong. Accelerating noisy VQE optimization with Gaussian processes. In *2022 IEEE International Conference on Quantum Computing and Engineering*, pages 215–225. IEEE, 2022. doi:[10.1109/QCE53715.2022.00041](https://doi.org/10.1109/QCE53715.2022.00041).
- [47] Quan Nguyen, Kaiwen Wu, Jacob Gardner, and Roman Garnett. Local Bayesian optimization via maximizing probability of descent. *Advances in Neural Information Processing Systems*, 35:13190–13202, 2022. URL <https://dl.acm.org/doi/10.5555/3600270.3601228>.
- [48] Christopher J Paciorek and Mark J Schervish. Spatial modelling using a new class of nonstationary covariance functions. *Environmetrics: The Official Journal of the International Environmetrics Society*, 17(5):483–506, 2006. doi:[10.1002/env.785](https://doi.org/10.1002/env.785).
- [49] Giulia Pedrielli and Szu Hui Ng. G-STAR: A new kriging-based trust region method for global optimization. In *2016 Winter Simulation Conference*, pages 803–814. IEEE, 2016. doi:[10.1109/WSC.2016.7822143](https://doi.org/10.1109/WSC.2016.7822143).
- [50] Victor Picheny and David Ginsbourger. A nonstationary space-time Gaussian process model for partially converged simulations. *SIAM/ASA Journal on Uncertainty Quantification*, 1(1):57–78, 2013. doi:[10.1137/120882834](https://doi.org/10.1137/120882834).
- [51] Victor Picheny, David Ginsbourger, Yann Richet, and Gregory Caplin. Quantile-based optimization of noisy computer experiments with tunable precision. *Technometrics*, 55(1):2–13, 2013. doi:[10.1080/00401706.2012.707580](https://doi.org/10.1080/00401706.2012.707580).
- [52] Victor Picheny, Tobias Wagner, and David Ginsbourger. A benchmark of kriging-based infill criteria for noisy optimization. *Structural and Multidisciplinary Optimization*, 48:607–626, 2013. doi:[10.1007/s00158-013-0919-4](https://doi.org/10.1007/s00158-013-0919-4).
- [53] John Preskill. Quantum computing in the NISQ era and beyond. *Quantum*, 2:79, August 2018. ISSN 2521-327X. doi:[10.22331/q-2018-08-06-79](https://doi.org/10.22331/q-2018-08-06-79). URL <http://dx.doi.org/10.22331/q-2018-08-06-79>.
- [54] Stefan Pricopie, Richard Allmendinger, Manuel López-Ibáñez, Clyde Fare, Matt Benatan, and Joshua Knowles. An adaptive approach to Bayesian optimization with setup switching costs. In Michael Affenzeller, Stephan M. Winkler, Anna V. Kononova, Heike Trautmann, Tea Tušar, Penousal Machado, and Thomas Bäck, editors, *Parallel Problem Solving from Nature – PPSN XVIII*, pages 340–355, Cham, 2024. Springer Nature Switzerland. ISBN 978-3-031-70068-2. doi:[10.1007/978-3-031-70068-2_21](https://doi.org/10.1007/978-3-031-70068-2_21).
- [55] Shyam Sundhar Ramesh, Pier Giuseppe Sessa, Andreas Krause, and Ilija Bogunovic. Movement penalized Bayesian optimization with application to wind energy systems. *Advances in Neural Information Processing Systems*, 35:27036–27048, 2022. URL <https://dlnext.acm.org/doi/10.5555/3600270.3602230>.

- [56] Carl E. Rasmussen and Christopher Williams. *Gaussian Processes for Machine Learning*. MIT Press, 2006. doi:[10.7551/mitpress/3206.001.0001](https://doi.org/10.7551/mitpress/3206.001.0001).
- [57] Rommel G Regis. Trust regions in Kriging-based optimization with expected improvement. *Engineering Optimization*, 48(6):1037–1059, 2016. doi:[10.1080/0305215X.2015.1082350](https://doi.org/10.1080/0305215X.2015.1082350).
- [58] Matthieu Sacher, Olivier Le Maitre, Régis Duvigneau, Frédéric Hauville, Mathieu Durand, and Corentin Lothodé. A non-nested infilling strategy for multifidelity based efficient global optimization. *International Journal for Uncertainty Quantification*, 11(1), 2021. doi:[10.1615/Int.J.UncertaintyQuantification.2020032982](https://doi.org/10.1615/Int.J.UncertaintyQuantification.2020032982).
- [59] Maria Laura Santoni, Elena Raponi, Renato De Leone, and Carola Doerr. Comparison of high-dimensional Bayesian optimization algorithms on BBOB. *ACM Transactions on Evolutionary Learning*, 4(3):1–33, 2024. doi:[10.1145/3670683](https://doi.org/10.1145/3670683).
- [60] Sara Shashaani, Fatemeh S. Hashemi, and Raghu Pasupathy. ASTRO-DF: A class of adaptive sampling trust-region algorithms for derivative-free stochastic optimization. *SIAM Journal on Optimization*, 28(4):3145–3176, January 2018. ISSN 1095-7189. doi:[10.1137/15m1042425](https://doi.org/10.1137/15m1042425). URL <http://dx.doi.org/10.1137/15M1042425>.
- [61] Edward Snelson and Zoubin Ghahramani. Sparse Gaussian processes using pseudo-inputs. *Advances in Neural Information Processing Systems*, 18, 2005. URL <https://dl.acm.org/doi/abs/10.5555/2976248.2976406>.
- [62] Edward Snelson and Zoubin Ghahramani. Variable noise and dimensionality reduction for sparse Gaussian processes. In *Proceedings of the Twenty-Second Conference on Uncertainty in Artificial Intelligence*, pages 461–468, 2006. URL <https://dl.acm.org/doi/10.5555/3020419.3020475>.
- [63] Jasper Snoek, Hugo Larochelle, and Ryan P Adams. Practical Bayesian optimization of machine learning algorithms. *Advances in Neural Information Processing Systems*, 25, 2012. URL <https://dl.acm.org/doi/10.5555/2999325.2999464>.
- [64] Ke Wang, Geoff Pleiss, Jacob Gardner, Stephen Tyree, Kilian Q Weinberger, and Andrew Gordon Wilson. Exact Gaussian processes on a million data points. *Advances in Neural Information Processing Systems*, 32, 2019. doi:[10.5555/3454287.3455599](https://doi.org/10.5555/3454287.3455599).
- [65] Wenjia Wang and Benjamin Haaland. Controlling sources of inaccuracy in stochastic kriging. *Technometrics*, 2019. doi:[10.1080/00401706.2018.1514328](https://doi.org/10.1080/00401706.2018.1514328).
- [66] Stefan M. Wild and Christine A. Shoemaker. Global convergence of radial basis function trust region derivative-free algorithms. *SIAM Journal on Optimization*, 21(3):761–781, 2011. doi:[10.1137/09074927X](https://doi.org/10.1137/09074927X).
- [67] Stefan M Wild, Rommel G Regis, and Christine A Shoemaker. ORBIT: Optimization by radial basis function interpolation in trust-regions. *SIAM Journal on Scientific Computing*, 30(6):3197–3219, 2008. doi:[10.1137/070691814](https://doi.org/10.1137/070691814).

- [68] Kaiwen Wu, Kyurae Kim, Roman Garnett, and Jacob Gardner. The behavior and convergence of local Bayesian optimization. *Advances in Neural Information Processing Systems*, 36, 2024. URL <https://dl.acm.org/doi/10.5555/3666122.3669337>.
- [69] Boya Zhang, Robert B Gramacy, Leah R Johnson, Kenneth A Rose, and Eric Smith. Batch-sequential design and heteroskedastic surrogate modeling for delta smelt conservation. *The Annals of Applied Statistics*, 16(2):816–842, 2022.
- [70] Leo Zhou, Sheng-Tao Wang, Soonwon Choi, Hannes Pichler, and Mikhail D. Lukin. Quantum approximate optimization algorithm: Performance, mechanism, and implementation on near-term devices. *Physical Review X*, 10(2), June 2020. ISSN 2160-3308. doi:10.1103/physrevx.10.021067. URL <http://dx.doi.org/10.1103/PhysRevX.10.021067>.

The submitted manuscript has been created by UChicago Argonne, LLC, Operator of Argonne National Laboratory (“Argonne”). Argonne, a U.S. Department of Energy Office of Science laboratory, is operated under Contract No. DE-AC02-06CH11357. The U.S. Government retains for itself, and others acting on its behalf, a paid-up nonexclusive, irrevocable worldwide license in said article to reproduce, prepare derivative works, distribute copies to the public, and perform publicly and display publicly, by or on behalf of the Government. The Department of Energy will provide public access to these results of federally sponsored research in accordance with the DOE Public Access Plan <http://energy.gov/downloads/doe-public-access-plan>.

A Sensitivity analysis of OGPIT’s parameters

We show the effect of modifying the parameters of the method compared to the given default values on the problems of Benchmark 1.

A.1 Effect of the trust region increase/decrease coefficient

The coefficient for decreasing the TR radius, γ_{dec} is studied in [Figure 9](#). There is no clear best value, while the smallest coefficient ($\gamma_{dec} = 0.6$) is the best only once, for the deterministic version, for the smallest gate. A larger value ($\gamma_{dec} = 0.9$) is sometimes better but the difference with the default is slight.

A.2 Parameter for the IMSE ratio

In Step 19 of [Algorithm 1](#), the variance of the mean needs to be 10 times larger than the mean predictive variance (IMSE) to allow for decreasing the TR radius. In [Figure 10](#), we study other values. Except for the deterministic version where it is not used, smaller values for the ratio (0.1 or 1) show a degraded performance and highlight the importance of preventing the decrease when the noise is dominating. The largest values, 100, gets slightly worse results than the default value.

A.3 Value of the minimal variance reduction

[Figure 11](#) deals with the imposed minimal variance reduction at the new design, T_a . The default value shows the best overall performance, while the largest value ($T_a = 0.5$) can be detrimental.

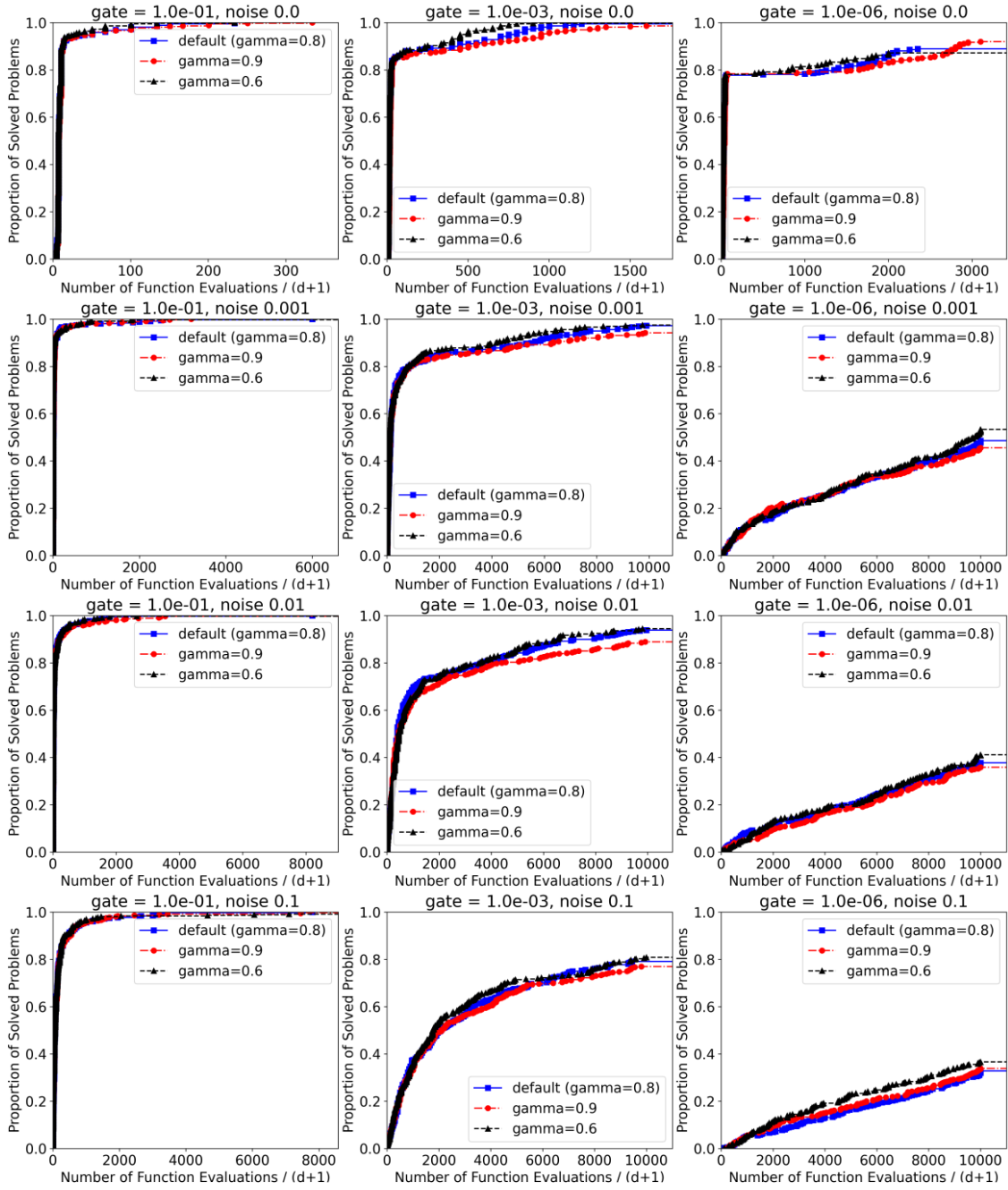


Figure 9: Data profiles for varying γ_{dec} , over 40 repetitions.

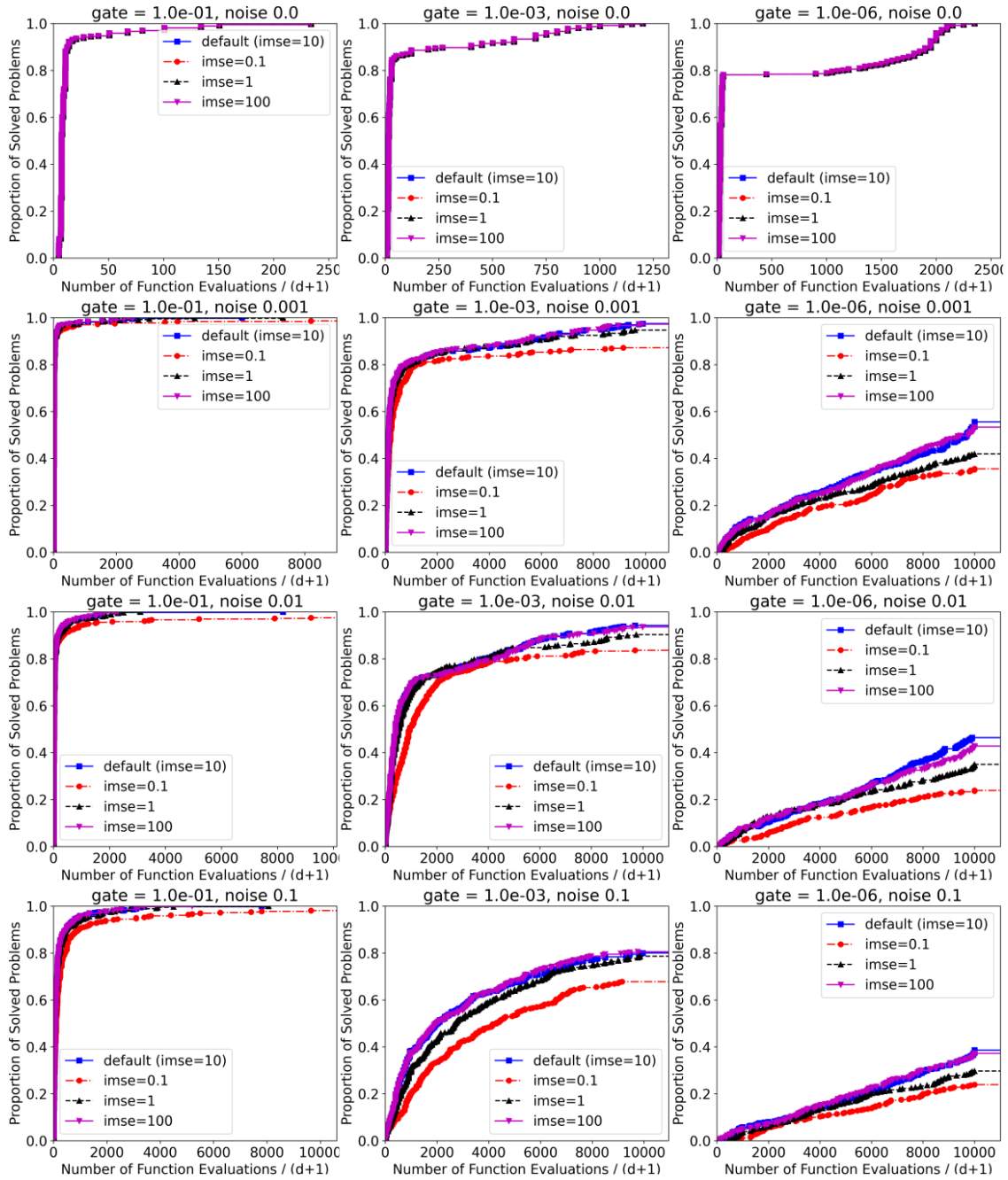


Figure 10: Data profiles for varying the IMSE - variance ratio, over 40 repetitions.

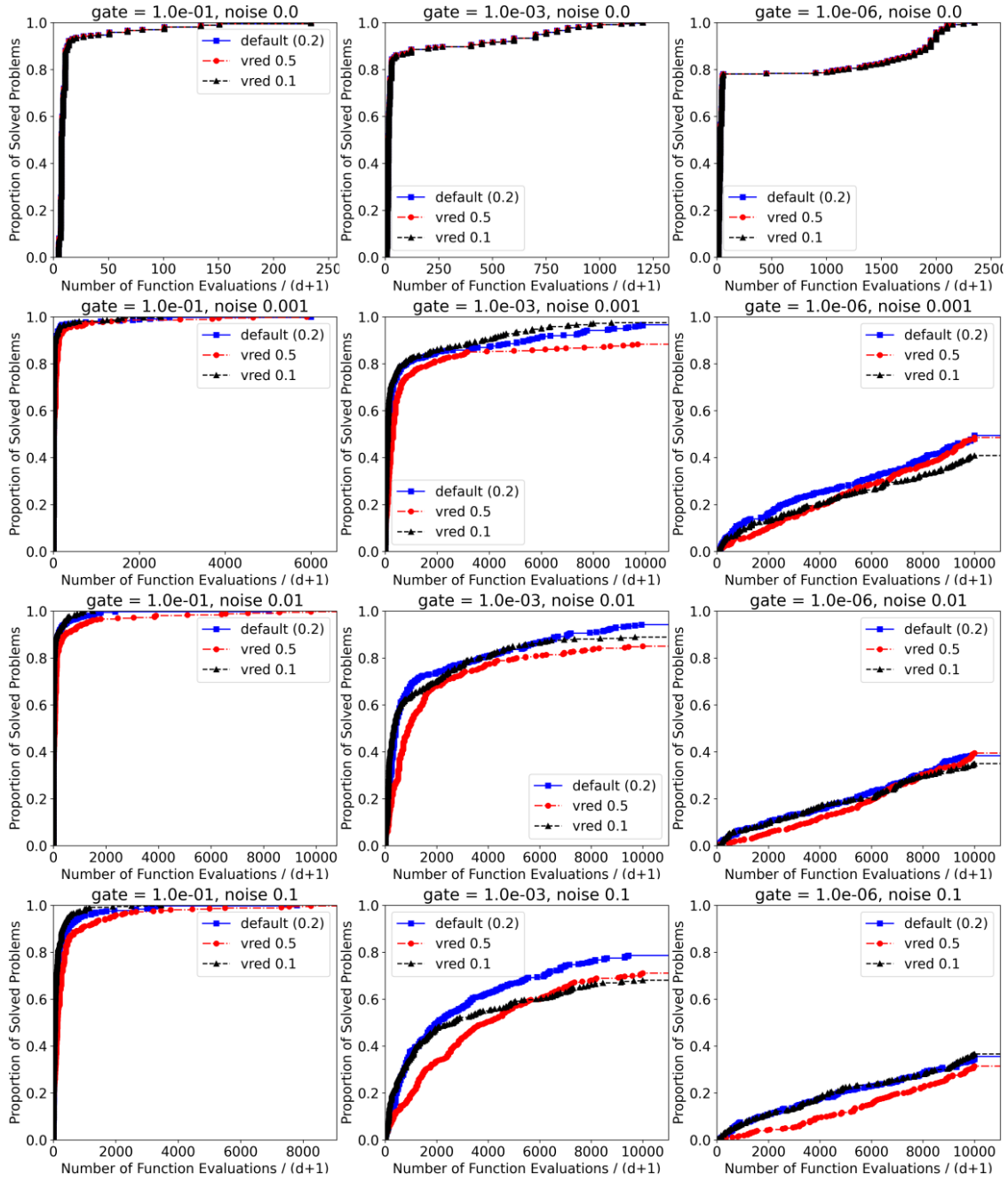


Figure 11: Data profiles with varying minimal variance reduction T_a .

A.4 Value of the predictive variance ratio

Figure 12 deals with the relative ratio of predictive variances between the center and new point. For the largest noise variance, higher values (9,16) than the default (4) may be more suitable, but not too large since, overall, 9 is slightly dominating 16 at the latest iterations.

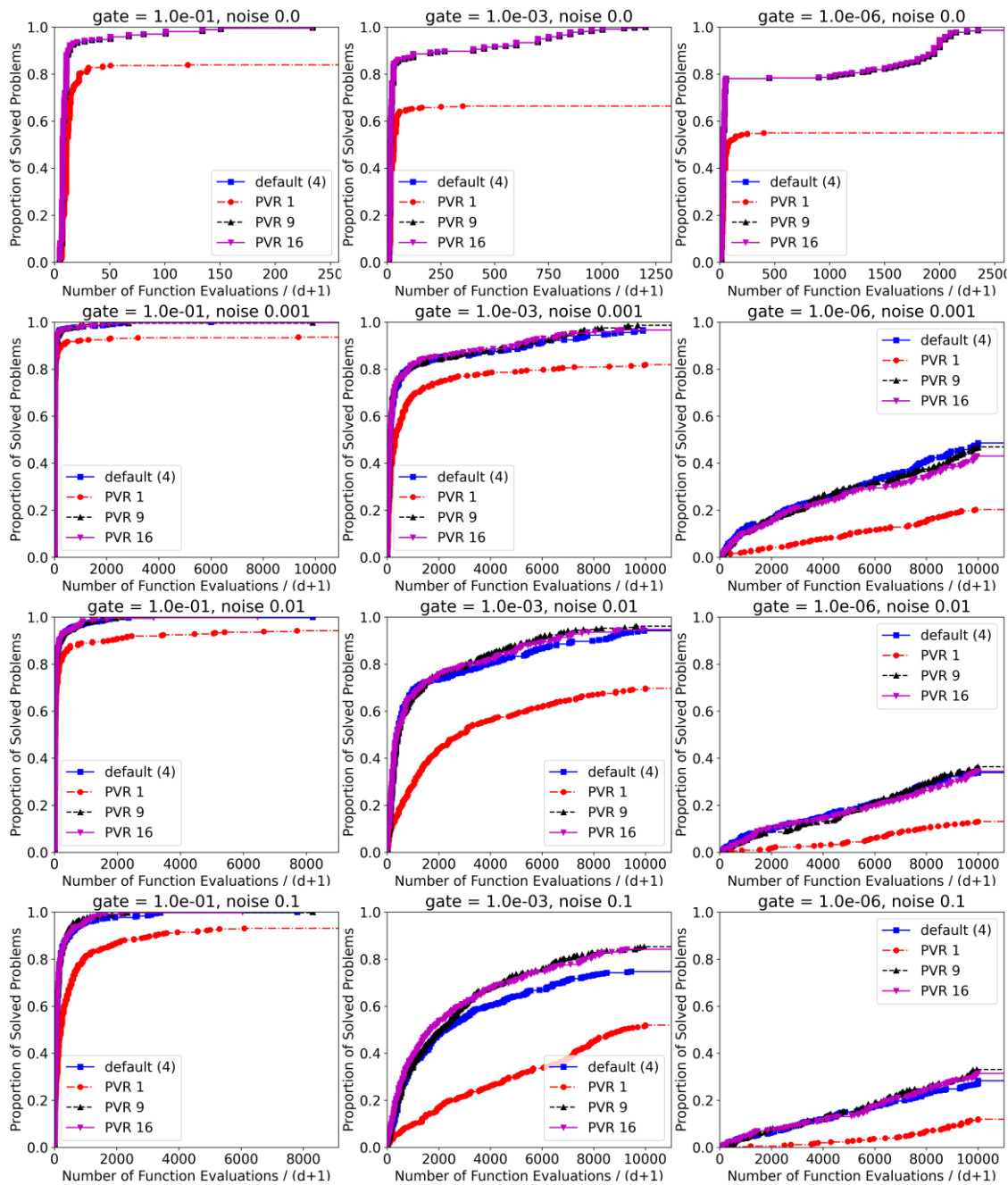


Figure 12: Data profiles with varying predictive variance ratio between \mathbf{x}_c and \mathbf{x}_{n+1} .

B Comparison to fixed replication budget

Compared to using a fixed replication budget, we illustrate the dynamic of the replication effort with OGPIT in Figure 13. It depends on the test function, but it is possible to see the effect of the dimension where the increase in the number of replication is delayed. The effect of the noise magnitude is visible mostly for the largest noise case. The lines are full as long as no run finished before this iteration, then dashed lines are used. It explains the more chaotic behavior at the latest iterations: there are less repetitions to average over and if the budget is almost exhausted, the number of replications at the last iteration may be small. The maximum replication budget p_{max} is set to 500, which is reached mostly on the latest iterations for a few functions.

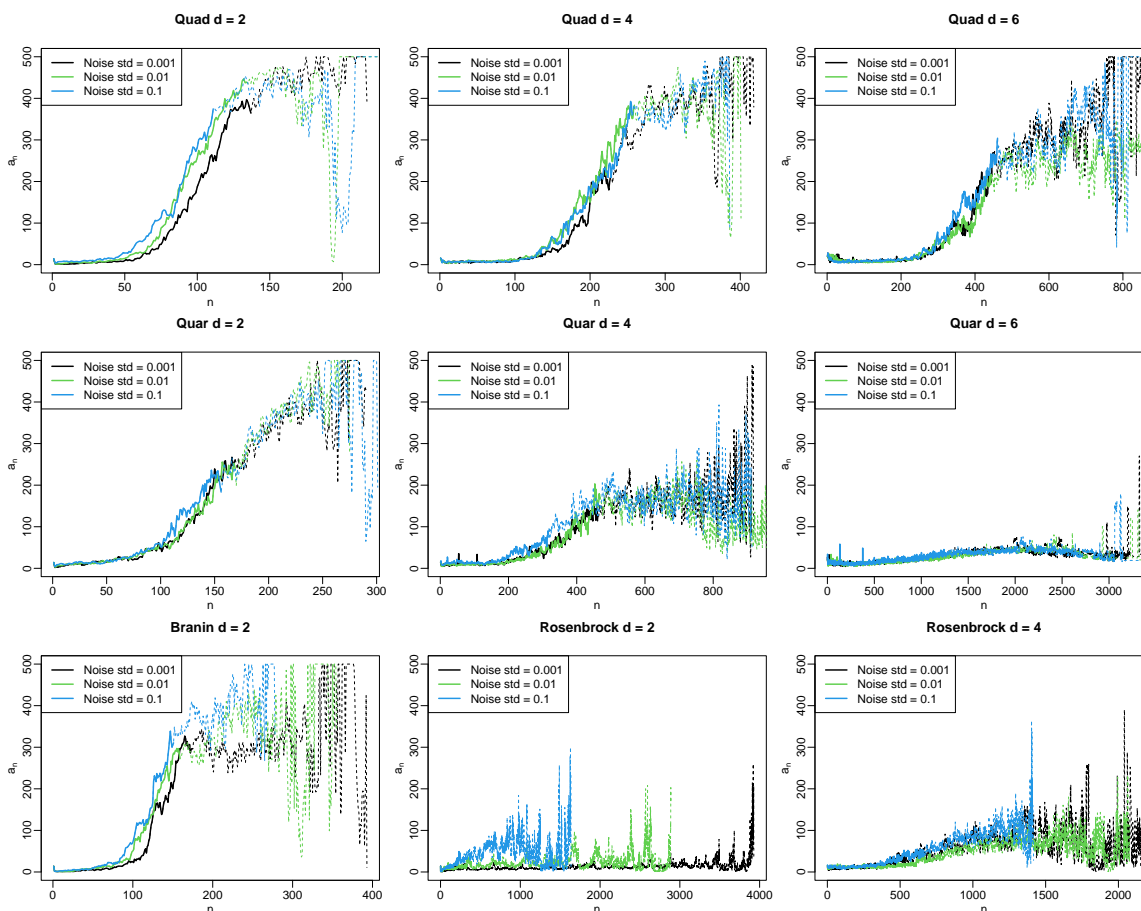


Figure 13: Average number of replication at each iteration over 40 repetitions on the Benchmark 1 test functions. Since the total budget may be reached earlier if more replications are done, dashed lines indicates that less than 40 repetitions are averaged over.

From the previous figure, setting an appropriate fixed replication number seems difficult. In Figure 14, we show that, indeed, fixing the replication budget is detrimental: it impacts the performance at the early iterations while more replicates are needed at the end (as can be seen especially in the middle column.)

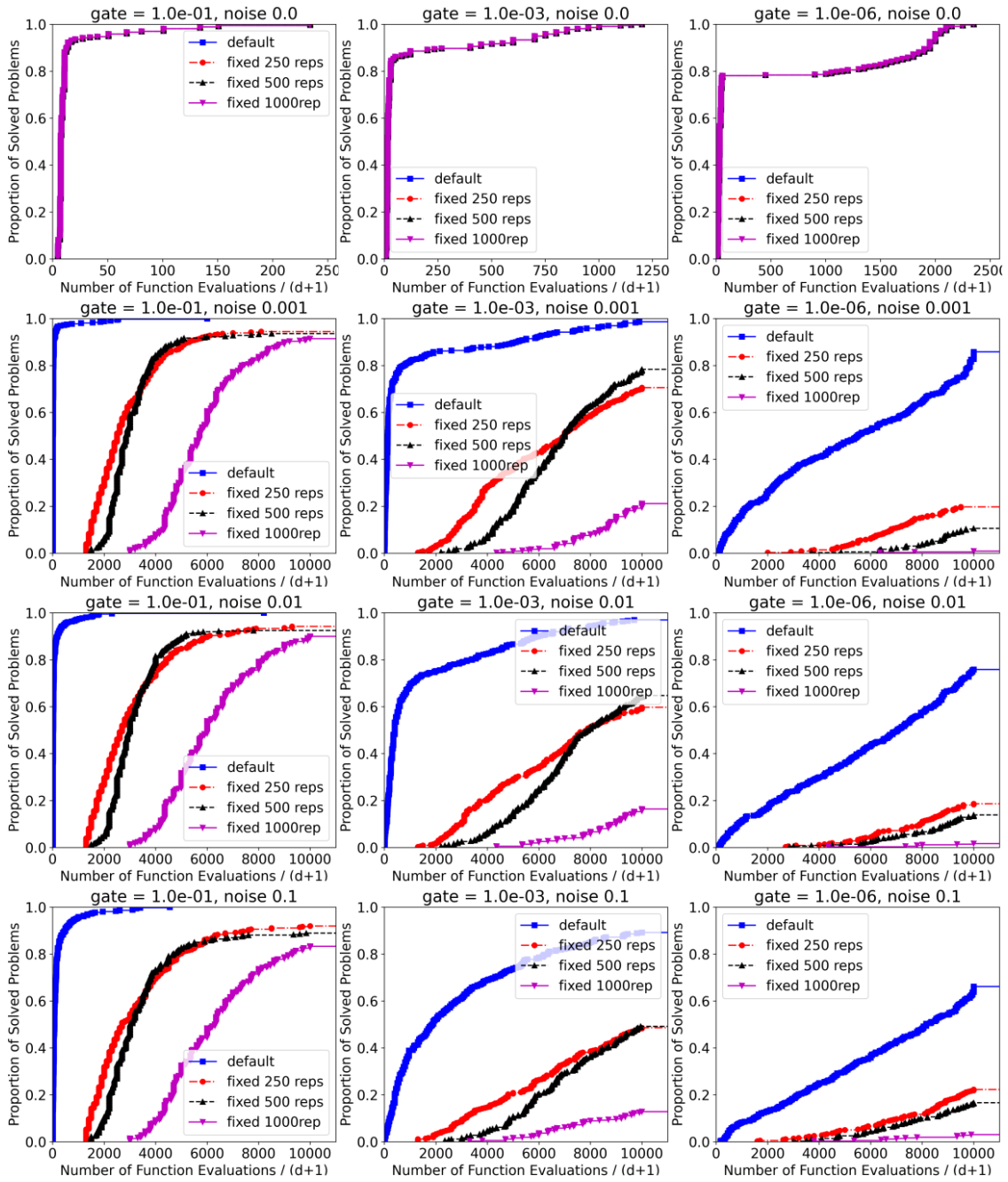


Figure 14: Data profiles with varying fixed replication budgets, over 40 repetitions.